Coronaviruses exploit a host cysteine-aspartic protease for efficient replication

Kwok-Yung Yuen (kyyuen@hku.hk)
The University of Hong Kong https://orcid.org/0000-0002-2083-1552

Hin Chu
University of Hong Kong

Yuxin Hou
The University of Hong Kong

Dong Yang
The University of Hong Kong

Lei Wen
The University of Hong Kong

Huiping Shuai
The University of Hong Kong

Terrence Tsz-Tai Yuen
The University of Hong Kong

Cun Li
The University of Hong Kong

Xiaoyu Zhao
The University of Hong Kong

Yixin Wang
The University of Hong Kong

Bingjie Hu
The University of Hong Kong

Xiner Huang
The University of Hong Kong

Yue Chai
The University of Hong Kong

Chaemin Yoon
The University of Hong Kong

Jian-Piao Cai
The University of Hong Kong

Vincent Poon
The University of Hong Kong

Chris Chan

The University of Hong Kong
Jinxia Zhang
Department of microbiology https://orcid.org/0000-0002-5087-3614
Shuofeng Yuan
University of Hong Kong
Ko-Yung Sit
The University of Hong Kong https://orcid.org/0000-0001-6289-663X
Dominic Chi-Chung Foo
The University of Hong Kong
Wing-Kuk Au
The University of Hong Kong
Kenneth Kak-Yuen Wong
The University of Hong Kong
Jie Zhou
University of Hong Kong https://orcid.org/0000-0002-2948-3873
Kin-Hang Kok
The University of Hong Kong https://orcid.org/0000-0003-3426-332X
Dong-Yan Jin
University of Hong Kong https://orcid.org/0000-0002-2778-3530
Jasper Chan
The University of Hong Kong https://orcid.org/0000-0001-6336-6657

Biological Sciences - Article

Keywords: Apoptosis Cascade, Pathogenesis Modulation, N Fragments, Caspase-6

Posted Date: March 26th, 2021

DOI: https://doi.org/10.21203/rs.3.rs-354943/v1

Version of Record: A version of this preprint was published at Nature on August 3rd, 2022. See the published version at https://doi.org/10.1038/s41586-022-05148-4.

Coronaviruses exploit a host cysteine-aspartic protease for efficient replication

Authors

Hin Chu[1,2,9,✉], Yuxin Hou[2,9], Dong Yang[2], Lei Wen[2], Huiping Shuai[2], Terrence Tsz-Tai Yuen[2], Cun Li[2], Xiaoyu Zhao[2], Yixin Wang[2], Bingjie Hu[2], Xiner Huang[2], Yue Chai[2], Chaemin Yoon[2], Jian-Piao Cai[2], Vincent Kwok-Man Poon[2], Chris Chung-Sing Chan[2], Anna Jinxia Zhang[1,2], Shuofeng Yuan[1,2], Ko-Yung Sit[3], Dominic Chi-Chung Foo[3], Wing-Kuk Au[3], Kenneth Kak-Yuen Wong[3], Jie Zhou[1,2], Kin-Hang Kok[1,2], Dong-Yan Jin[4], Jasper Fuk-Woo Chan[1,2,5,6,7,8,✉], Kwok-Yung Yuen[1,2,5,6,7,8,✉]

Affiliations

[1]State Key Laboratory of Emerging Infectious Diseases, Li Ka Shing Faculty of Medicine, The University of Hong Kong, Pokfulam, Hong Kong Special Administrative Region, China.

[2]Department of Microbiology, Li Ka Shing Faculty of Medicine, The University of Hong Kong, Pokfulam, Hong Kong Special Administrative Region, China.

[3]Department of Surgery, Li Ka Shing Faculty of Medicine, The University of Hong Kong, Pokfulam, Hong Kong Special Administrative Region, China.

[4]School of Biomedical Sciences, Li Ka Shing Faculty of Medicine, The University of Hong Kong, Pokfulam, Hong Kong Special Administrative Region, China.

[5]Carol Yu Centre for Infection, Li Ka Shing Faculty of Medicine, The University of Hong Kong, Pokfulam, Hong Kong Special Administrative Region, China.

[6]Department of Microbiology, Queen Mary Hospital, Pokfulam, Hong Kong Special Administrative Region, China.

[7]Department of Clinical Microbiology and Infection Control, The University of Hong Kong-Shenzhen Hospital, Shenzhen, Guangdong Province, China.

[8]Hainan Medical University-The University of Hong Kong Joint Laboratory of Tropical Infectious Diseases, The University of Hong Kong, Pokfulam, Hong Kong Special Administrative Region, China.

[9]These authors contributed equally to this work.

✉**Corresponding authors:** Kwok-Yung Yuen (kyyuen@hku.hk), Jasper Fuk-Woo Chan (jfwchan@hku.hk), and Hin Chu (hinchu@hku.hk).

Summary

Highly pathogenic coronaviruses including severe acute respiratory syndrome coronavirus 2 (SARS-CoV-2)[1,2], Middle East respiratory syndrome coronavirus (MERS-CoV)[3,4], and SARS-CoV-1[5] vary in their transmissibility and pathogenicity. However, infection by all three viruses result in substantial apoptosis in cell culture[6-8] and in patient samples[9-11], suggesting a potential link between apoptosis and the pathogenesis of coronaviruses. To date, the underlying mechanism of how apoptosis modulates coronavirus pathogenesis is unknown. Here we show that a cysteine-aspartic protease of the apoptosis cascade, caspase-6, serves as an essential host factor for efficient coronavirus replication. We demonstrate that caspase-6 cleaves coronavirus nucleocapsid (N) proteins, generating N fragments that serve as interferon (IFN) antagonists, thus facilitating virus replication. Inhibition of caspase-6 substantially attenuates the lung pathology and body weight loss of SARS-CoV-2-infected golden Syrian hamsters and improves the survival of mouse-adapted MERS-CoV (MERS-CoV_{MA})-infected human DPP4 knock-in (hDPP4 KI) mice. Overall, our study reveals how coronaviruses exploit a component of the host apoptosis cascade to facilitate their replication. These results further suggest caspase-6 as a potential target of intervention for the treatment of highly pathogenic coronavirus infections including COVID-19 and MERS.

Seven coronaviruses are known to infect humans. Among them, three highly pathogenic coronaviruses, including severe acute respiratory syndrome coronavirus 2 (SARS-CoV-2)[1,2], Middle East respiratory syndrome coronavirus (MERS-CoV)[3,4], and SARS-CoV-1[5], have emerged over the last two decades and have dramatically impacted the global public health of the human populations[12]. These highly pathogenic coronaviruses vary in their transmissibility and pathogenicity with underlying mechanism remains largely unexplained[13]. A common feature of these coronaviruses is their propensity to induce apoptosis in the infected target cells. SARS-CoV-1 infection induced apoptosis in cell culture and infected patients[9,10]. MERS-CoV triggered severe apoptosis in lung epithelial cells[6], primary T cells[7], and infected animals[14]. More recently, SARS-CoV-2-induced apoptosis was similarly documented in infected human tracheobronchial epithelial cells[8], lungs of infected hamsters[15], and lung specimens of Coronavirus Disease 2019 (COVID-19) patients[11]. These findings suggest a role of apoptosis in the pathogenesis of coronaviruses. In line with these observations, we recently demonstrated that inhibition of apoptosis with a pan-caspase inhibitor significantly attenuated MERS-CoV replication[14], suggesting a previously unrecognized connection between the apoptosis cascade and coronavirus replication.

In this study, we further investigated how apoptosis modulates coronavirus replication. Our results identify caspase-6, which is a cysteine-aspartic protease serving as an executor caspase of the apoptosis cascade, as a novel host factor that facilitates coronavirus replication. *In vitro* inhibition of caspase-6 reduces the replication of all evaluated human pathogenic coronaviruses including MERS-CoV, SARS-CoV-2, SARS-CoV-1, human coronavirus (HCoV)-229E, and HCoV-OC43. In human DPP4 knock-in (hDPP4 KI) mice, caspase-6 inhibition attenuates the replication of mouse-adapted MERS-CoV (MERS-CoV_{MA}) and significantly improves the survival of infected mice. Similarly, caspase-6 inhibition reduces SARS-CoV-2 replication in lungs of golden Syrian hamsters and markedly

ameliorates lung pathology, leading to significantly improved body weight in the infected hamsters. Mechanistically, we demonstrate that caspase-6 cleaves coronavirus N proteins and generates N fragments, which subsequently serve as interferon (IFN) antagonists that promote efficient virus replication. Importantly, caspase-6-mediated N cleavage and its associated IFN antagonism are conserved among all evaluated human-pathogenic coronaviruses. Overall, our study reveals a novel mechanism on how human-pathogenic coronaviruses exploit a component of the apoptosis cascade for their efficient replication. Caspase-6 inhibition can be further explored as an intervention strategy for coronavirus infections including MERS and COVID-19.

Results

Inhibition of caspase-6 limits coronavirus replication

We recently demonstrated that MERS-CoV infection triggered substantial apoptosis while inhibition of apoptosis with the pan-caspase inhibitor, z-VAD-fmk, significantly limited MERS-CoV replication (**Fig. 1a,b**)[14]. Interestingly, z-VAD-fmk similarly limited the replication of other human pathogenic coronaviruses including SARS-CoV-2, SARS-CoV-1, HCoV-229E, and HCoV-OC43 (**Fig. 1b**), suggesting that the dependency on apoptosis or caspase activity for efficient virus replication is a conserved mechanism for coronaviruses. Caspases are cysteine-aspartic proteases that regulate the host apoptosis cascade[16]. To investigate which caspase is most responsible for modulating coronavirus replication, we used MERS-CoV as a model virus and evaluated virus replication in the presence of specific inhibitors against individual caspases. Our results revealed that caspase-6 inhibition most dramatically limited MERS-CoV replication (**Fig. 1c,d**). The inhibitory effect on MERS-CoV replication by caspase-6 inhibition was conserved across different cell types with the exception of VeroE6 cells (**Extended Data Fig. 1**). Importantly, inhibition of caspase-6 with

its specific inhibitor, z-VEID-fmk, attenuated the replication of all evaluated coronaviruses including that of SARS-CoV-2 and SARS-CoV-1, but did not impact the replication of influenza virus (H1N1) or enterovirus (enterovirus A71) (**Fig. 1e**). According to RT-qPCR and $TCID_{50}$ assays, the IC_{50} of z-VEID-fmk against coronaviruses ranged from 3.3μM for SARS-CoV-2 to 21.1μM for MERS-CoV in the cell lysate samples and 1.2μM for SARS-CoV-2 to 30.6μM for HCoV-OC43 in the supernatant samples, respectively (**Fig. 1f**).

Next, we used MERS-CoV and SARS-CoV-2 as model coronaviruses and evaluated the impact of caspase-6 inhibition on coronavirus replication in infected human *ex vivo* lung tissues, human intestinal organoids, and animals. In human lung tissues, caspase-6 inhibition with z-VEID-fmk significantly reduced MERS-CoV nucleocapsid (N) protein and gene expression (**Fig. 2a,b**). Similarly, z-VEID-fmk inhibited MERS-CoV replication in human intestinal organoids and inhibited the production of infectious virus particles by approximately 80% ($p<0.0001$) at 24 hours post infection (hpi) (**Fig. 2c-f**). Caspase-6 is largely conserved among mammals and the z-VEID-fmk binding pocket is conserved among humans, mice, and hamsters, allowing us to evaluate the effect of caspase-6 inhibition with z-VEID-fmk in these animal models (**Extended Data Fig. 2**). To evaluate the impact of caspase-6 inhibition on MERS-CoV replication *in vivo*, we infected human DPP4 knock-in (hDPP4 KI) mice with mouse adapted MERS-CoV ($MERS\text{-}CoV_{MA}$)[17] and treated the mice with z-VEID-fmk or DMSO (**Fig. 2g**). Our results demonstrated that z-VEID-fmk effectively reduced $MERS\text{-}CoV_{MA}$ replication in the lungs of the infected mice at both day 2 and day 4 post infection (**Fig. 2h-j**), and significantly attenuated the expression of pro-inflammatory cytokines and chemokines (**Fig. 2k and Extended Data Fig. 3**). Importantly, the z-VEID-fmk treatment largely inhibited body weight loss and significantly improved the survival of the infected hDPP4 KI mice from 33.3% to 80% (3/9 vs 8/10; $p=0.0388$) (**Fig. 2l,m**).

We next asked whether z-VEID-fmk could similarly inhibit SARS-CoV-2 replication *in vivo*. To this end, we infected golden hamsters with SARS-CoV-2 through the intranasal route and treated the hamsters with z-VEID-fmk or DMSO (**Fig. 3a**). Our results demonstrated that caspase-6 inhibition with z-VEID-fmk significantly reduced SARS-CoV-2 replication in the hamster lungs (**Fig. 3b,c**) including small airways (**Fig. 3d**) and alveoli (**Fig. 3e**), and ameliorated the expression of virus-induced pro-inflammatory cytokines and chemokines (**Fig. 3f**). The attenuated virus replication and expression of pro-inflammatory markers resulted in significant improvements of the body weight of the infected hamsters (**Fig. 3g**). In addition, we harvested lung tissues from the hamsters at day 4 post infection to evaluate histological changes. Infected lungs from hamsters in the mock treatment group showed severe bronchiolar epithelial cell death and desquamation, extensive alveolar space mononuclear cell infiltration, protein rich fluid exudation, alveolar haemorrhage, and severe destruction of alveolar structure. Pulmonary blood vessel wall inflammation and endothelium infiltration were frequently observed (**Fig. 3h, middle panels**). These histopathological changes were consistent with what we previously reported in SARS-CoV-2-infected golden hamsters[15]. In contrast, in the lungs of z-VEID-fmk-treated hamsters, all categories of tissue damage, including bronchiolitis, alveolitis and vasculitis, were significantly ameliorated. In these animals, we observed a mild degree of bronchiolar epithelium desquamation, focal alveolar septal congestion, localized infiltration or hemorrhage, and mild perivascular infiltration. At the same time, the z-VEID-fmk treatment dramatically inhibited alveolar space immune cells infiltration (**Fig. 3h, bottom panels**). In order to quantitatively evaluate the severity of lung damage, we performed semi-quantitative histopathological examination of the bronchioles, alveoli, and blood vessels using our previously described methods[18]. According to the histopathological scores, the z-VEID-fmk treatment significantly ameliorated lung damage in the infected hamsters (**Fig. 3i**). Taken together, our results

158 demonstrate that caspase-6 inhibition attenuates coronavirus replication in cell culture,
159 human lung tissue, organoid, and animal settings.
160
161 **Caspase-6 cleaves nucleocapsid (N) protein and modulates coronavirus**
162 **replication at a post-entry step**
163 Next, we seek to understand the role of caspase-6 in coronavirus replication. Using MERS-
164 CoV as a model, we first assessed the effect of z-VEID-fmk in a time-of-addition assay,
165 which showed that z-VEID-fmk added during MERS-CoV inoculation did not reduce virus
166 replication (**Fig. 4a**). Consistent with this finding, MERS-CoV entry in caspase-6-stable
167 knockdown A549 and BEAS2B cells was not compromised (**Fig. 4b** and **Extended Data**
168 **Fig. 4a**), confirming the notion that caspase-6 did not play a role in MERS-CoV entry. Next,
169 we evaluated virus gene expression in caspase-6 stable knockdown cells harvested at 24 hpi.
170 Among these samples, MERS-CoV replication was significantly reduced in the presence of
171 caspase-6 knockdown (**Fig. 4c**). The role of caspase-6 on MERS-CoV replication was further
172 investigated in human primary monocyte-derived macrophages (MDMs). In these cells,
173 transient depletion of caspase-6 with siRNA markedly reduced MERS-CoV replication in
174 both cell lysates and supernatant samples (**Fig. 4d** and **Extended Data Fig. 4b**). In addition
175 to the gene depletion studies, we examined MERS-CoV replication in caspase-6-
176 overexpressed cells. Our results demonstrated that caspase-6 but not caspase-3
177 overexpression efficiently promoted MERS-CoV replication (**Fig. 4e,f**). Thus, these results
178 suggest that caspase-6 is required for efficient MERS-CoV replication at a post entry step.
179 Together with caspase-3 and caspase-7, caspase-6 is one of the three executor caspases that
180 execute apoptosis by proteolytic cleavage of host substrates[19]. Caspase-6 is cleavage
181 activated when apoptosis is induced but can also undergo autoactivation (**Extended Data**
182 **Fig. 5**)[20]. As a cysteine-aspartic protease, we speculate that caspase-6 may modulate

coronavirus replication by acting on a viral component. To this end, we co-expressed caspase-6 with various MERS-CoV components and evaluated viral protein cleavage by caspase-6 when apoptosis was induced. In these assays, we used staurosporine (STS) to trigger apoptosis to mimic the apoptotic environment in MERS-CoV-infected cells. Intriguingly, our results demonstrated that caspase-6 mediated the cleavage of the viral N protein but not other viral components (**Fig. 4g** and **Extended Data Fig. 6**). Cleavage of N was completely abolished in the presence of the specific caspase-6 inhibitor, z-VEID-fmk, suggesting that the cleavage is caspase-6 specific (**Fig. 4g**). Importantly, N cleavage was readily detected in cells infected by MERS-CoV (**Fig. 4h**), and was similarly inhibited by caspase-6 inhibition in the infected cells (**Fig. 4i**). In addition, N was only cleaved by capsase-6, but not by the key executor caspase, caspase-3 (**Fig. 4j**). Together, these results demonstrate that caspase-6 specifically cleaves MERS-CoV N and modulates virus replication at a post entry step.

Caspase-6-mediated N cleavage modulates interferon response and is conserved across human-pathogenic coronaviruses

Next, we seek to further investigate how caspase-6-mediated N cleavage modulates coronavirus replication. We demonstrated earlier that caspase-6 inhibition attenuated MERS-CoV replication in all evaluated cell types with the exception of VeroE6 (**Extended Data Fig. 1**), which is deficient in interferon (IFN) signaling due to a homozygous deletion in the type-I IFN gene cluster[21,22]. These results hinted that caspase-6-mediated N cleavage might modulate coronavirus replication through regulating IFN signaling. To test this hypothesis, we evaluated the role of caspase-6 and MERS-CoV N on regulating IFN response with IFN-β-reporter assays. Interestingly, our results demonstrated that MERS-CoV N co-expressed with caspase-6 suppressed IFN-β-reporter activation in a dose-dependent manner (**Fig. 5a**). In

parallel, co-expression of caspase-3 and MERS-CoV N or caspase-6 and MERS-CoV envelope (E) protein did not significantly impact IFN-β-reporter activation (**Fig 5b**). In addition to IFN-β-reporter activity, co-expression of caspase-6 and MERS-CoV N similarly reduced the expression of IFN-β and representative interferon-stimulated genes (ISGs) including IFIT1, IFIT2, IFIT3, IFITM3, TRIM22, and OAS1 (**Fig. 5c** and **Extended Data Fig. 7**). Recent studies have reported MERS-CoV ORF4a, ORF4b, and membrane (M) protein as potent IFN antagonists[23-25]. Our data showed that caspase-6 did not modulate the IFN antagonism of these known IFN antagonists (**Fig. 5d**). Importantly, our further investigations demonstrated that caspase-6 similarly mediated N cleavage of other human pathogenic coronaviruses, including that of SARS-CoV-2 and SARS-CoV-1 (**Fig. 5e**), which is in agreement with our earlier findings that caspase-6 inhibition attenuated the replication of these coronaviruses (**Fig. 1e,f**). We next expressed the N genes of these coronaviruses together with caspase-6, which revealed that the co-expression of coronavirus N with caspase-6 antagonized IFN-β-reporter activation and reduced the expression of representative ISGs including IFIT3 and OAS1 (**Fig. 5f,g**). Collectively, these results suggest that caspase-6-mediated N cleavage modulates coronavirus replication by regulating IFN signaling.

To further explain how caspase-6-mediated N cleavage regulates IFN response, we analyzed the potential caspase-6 cleavage sites on MERS-CoV N based on known caspase-6 substrate specificity[26] and the size of the cleavage fragments, and generated the corresponding N mutants that potentially interfered with caspase-6 cleavage (**Fig. 6a**). Western blot-based cleavage assays demonstrated that caspase-6-mediated cleavage was abolished for the $T^{239}KKA^{242}$ mutant, suggesting that caspase-6 cleaves MERS-CoV N at the $T^{239}KKD^{242}$ motif (**Fig. 6b**). Interestingly, the $T^{239}KKD^{242}$ motif is located within the intrinsically disordered region (IDR) of MERS-CoV N that bridges the N-terminal domain and C-terminal domain of N, which are structurally conserved among coronaviruses[27]. Similar putative

caspase-6 cleavage motifs are also present in the IDR of N of other human-pathogenic coronaviruses (**Extended Data Table. 1**). In IFN-β-reporter assays, caspase-6 and N-mediated IFN antagonism was attenuated when $T^{239}KKA^{242}$ was expressed in place of the wildtype N (**Fig. 6c**). These findings suggested that caspase-6-mediated MERS-CoV N cleavage is essential for its IFN antagonism. Next, we generated the N(1-241) and N(242-413) fragments that mimicked the N cleavage products (**Fig. 6a**). In Western blots, we showed that the two fragments were no longer cleaved by caspase-6 (**Fig. 6d**). Consistent with this result, in IFN-β-reporter assays, the two N cleavage products individually limited IFN-β-reporter activity but were no longer modulated by caspase-6 (**Fig. 6e**). To dissect how the N fragments modulate IFN signaling, we explored their capacity of interacting with different components of the IFN signaling pathway with co-immunoprecipitation assays. Our results demonstrated that both N(1-241) and N(242-413) fragments interacted with IRF3 but not other components of the IFN signaling pathway (**Fig. 6f** and **Extended Data Fig. 8**). In poly(I:C)-treated 293T cells, IRF3 translocated to the cell nuclei regardless of MERS-CoV N expression. In stark contrast, both N(1-241) and N(242-413) fragments co-localized with IRF3 and abolished its nucleus translocation (**Fig. 6g**). Taken together, our study identifies caspase-6-mediated N cleavage as a novel mechanism that serves to dampen the host IFN response for efficient coronavirus replication. Inhibition of caspase-6 markedly attenuates coronavirus replication and ameliorates coronavirus-induced lung pathology *in vivo*, suggesting that caspase-6 inhibition should be further explored as an option for the treatment of highly pathogenic coronaviruses (**Extended Data Fig. 9**).

Discussion

In this study, we reveal caspase-6 as an essential host factor for efficient coronavirus replication. Caspase-6 inhibition limits the replication of all evaluated human-pathogenic

coronaviruses including MERS-CoV, SARS-CoV-2, SARS-CoV-1, HCoV-229E, and HCoV-OC43. In addition, caspase-6 inhibition significantly lowers the replication of highly pathogenic coronaviruses including MERS-CoV and SARS-CoV-2 *in vivo*, which improves the survival of MERS-CoV_{MA}-infected hDPP4 KI mice and attenuates the body weight loss and lung pathology of SARS-CoV-2-infected golden Syrian hamsters. Mechanistically, caspase-6 mediates the cleavage of coronavirus N protein. The N cleavage products serve as IFN antagonists and interfere with activation of IFN signaling, which reduces the expression of ISGs, leading to efficient coronavirus replication. Overall, our study reveals a novel mechanism for efficient coronavirus replication. Upon coronavirus infection, the host initiates apoptosis to eliminate infected cells and terminate virus propagation. At the same time, coronaviruses exploit a component of the activated apoptosis cascade to facilitate virus replication in order to maximize virus production before the cells are obliterated due to apoptosis induction. This is an elegant example of virus-host interaction that exemplifies the long-standing arms race between humans and coronaviruses.

The replication of coronaviruses including MERS-CoV and SARS-CoV-2 is known to depend on a host serine protease, transmembrane protease serine 2 (TMPRSS2), which cleavage activates the spike (S) protein of coronaviruses for efficient entry and replication[28,29]. In contrast, the role of host cysteine-aspartic protease on coronavirus replication has not been explored. Previous studies have suggested that influenza viruses require a host cysteine-aspartic protease, caspase-3, for efficient translocation of viral ribonucleoprotein (RNP) complexes across the nuclear membrane, which is essential for efficient virus replication[30,31]. In the current study, we show that caspase-6 but not caspase-3 facilitates coronavirus replication. Caspase-6 is most known for its role as an executor caspase and its catalytic role in neurodegeneration in Huntington's and Alzheimer's disease[32]. Here, we demonstrate that caspase-6 mediates efficient coronavirus replication by cleaving

coronavirus N proteins, which in turn serve as IFN antagonists that block IFN activation. Importantly, inhibiting caspase-6 attenuates virus replication and disease severity in highly pathogenic coronavirus-infected mice and hamsters. These findings suggest that in addition to the serine protease TMPRSS2, inhibiting the cysteine-aspartic protease caspase-6 should also be further explored as a therapeutic option against the infection by highly pathogenic coronaviruses including SARS-CoV-2.

A large body of studies identified viral components of different viruses on their potential role as IFN antagonists by individually expressing the viral components. Our study reveals host proteases as previously unappreciated factors that can modulate viral antagonism. Taking this new knowledge into consideration, our current understanding on viral components that antagonize IFN signaling may be incomplete since viral components may be processed by host proteases, thus modulating their capacity in interacting with the host IFN signaling pathways.

In the current study, we demonstrated that caspase-6 mediated the cleavage of N protein of all evaluated human pathogenic coronaviruses including MERS-CoV, SARS-CoV-2, SARS-CoV-1, HCoV-229E, HCoV-OC43, and HCoV-NL63. In addition to these human pathogenic coronaviruses, the N protein of transmissible gastroenteritis coronavirus (TGEV) and porcine epidemic diarrhea virus (PEDV), which are alphacoronaviruses that infect pigs, can also be cleaved by caspase-6 [33,34]. To this end, it will be interesting to further investigate if the caspase-6-mediated N cleavage mechanism and its associated IFN antagonism can be further generalized beyond human-pathogenic coronaviruses to other members of the coronavirus family.

Acknowledgements

This study was partly supported by the Health and Medical Research Fund (CID-HKU1-5 and 16150572), the Food and Health Bureau, the Government of the Hong Kong Special Administrative Region; the Consultancy Service for Enhancing Laboratory Surveillance of Emerging Infectious Diseases and Research Capability on Antimicrobial Resistance for Department of Health of the Hong Kong Special Administrative Region Government; and Innovation and Technology Fund (ITF), the Government of the Hong Kong Special Administrative Region; and the donations of Richard Yu and Carol Yu, the Shaw Foundation of Hong Kong, Michael Seak-Kan Tong, May Tam Mak Mei Yin, Lee Wan Keung Charity Foundation Limited, Respiratory Viral Research Foundation Limited, Hui Ming, Hui Hoy and Chow Sin Lan Charity Fund Limited, Chan Yin Chuen Memorial Charitable Foundation, Marina Man-Wai Lee, the Hong Kong Hainan Commercial Association South China Microbiology Research Fund, the Jessie & George Ho Charitable Foundation, Perfect Shape Medical Limited, Kai Chong Tong, Tse Kam Ming Laurence, Foo Oi Foundation Limited, Betty Hing-Chu Lee, Ping Cham So, and Lo Ying Shek Chi Wai Foundation. The funding sources had no role in the study design, data collection, analysis, interpretation, or writing of the report.

Author contributions

H.C. and Y.H. contributed equally to this work. H.C., J.F.W.C., and K.Y.Y. designed the study. H.C., Y.H., D.Y., L.W., H.S., T.T.T.Y., X.Z., C.L., Y.W., B.H., X.H., Y.C., C.Y., J.P.C., A.J.Z., S.Y., K.Y.S., I.H.Y.C., W.K.A., K.K.Y.W., J.Z., D.Y.J., K.H.K. performed experiments, analyzed data, or provided key resources. H.C., Y.H., J.F.W.C., and K.Y.Y. wrote the manuscript.

Correspondence and requests for materials should be addressed to H.C., J.F.W.C., or K.Y.Y.

Data availability

The data that support the findings of this study are available from the corresponding authors upon reasonable request.

Competing Interests

JFW Chan has received travel grants from Pfizer Corporation Hong Kong and Astellas Pharma Hong Kong Corporation Limited, and was an invited speaker for Gilead Sciences Hong Kong Limited and Luminex Corporation. The other authors declared no conflict of interests. The funding sources had no role in study design, data collection, analysis or interpretation or writing of the report.

References

1 Chan, J. F. *et al.* A familial cluster of pneumonia associated with the 2019 novel coronavirus indicating person-to-person transmission: a study of a family cluster. *Lancet* **395**, 514-523, doi:10.1016/S0140-6736(20)30154-9 (2020).

2 Zhou, P. *et al.* A pneumonia outbreak associated with a new coronavirus of probable bat origin. *Nature* **579**, 270-273, doi:10.1038/s41586-020-2012-7 (2020).

3 Zaki, A. M., van Boheemen, S., Bestebroer, T. M., Osterhaus, A. D. & Fouchier, R. A. Isolation of a novel coronavirus from a man with pneumonia in Saudi Arabia. *N Engl J Med* **367**, 1814-1820, doi:10.1056/NEJMoa1211721 (2012).

4 Chan, J. F. *et al.* Middle East respiratory syndrome coronavirus: another zoonotic betacoronavirus causing SARS-like disease. *Clin Microbiol Rev* **28**, 465-522, doi:10.1128/CMR.00102-14 (2015).

5 Peiris, J. S. *et al.* Coronavirus as a possible cause of severe acute respiratory syndrome. *Lancet* **361**, 1319-1325, doi:10.1016/s0140-6736(03)13077-2 (2003).

6 Tao, X. *et al.* Bilateral entry and release of Middle East respiratory syndrome coronavirus induces profound apoptosis of human bronchial epithelial cells. *J Virol* **87**, 9953-9958, doi:10.1128/JVI.01562-13 (2013).

7 Chu, H. *et al.* Middle East Respiratory Syndrome Coronavirus Efficiently Infects Human Primary T Lymphocytes and Activates the Extrinsic and Intrinsic Apoptosis Pathways. *J Infect Dis* **213**, 904-914, doi:10.1093/infdis/jiv380 (2016).

8 Zhu, N. *et al.* Morphogenesis and cytopathic effect of SARS-CoV-2 infection in human airway epithelial cells. *Nat Commun* **11**, 3910, doi:10.1038/s41467-020-17796-z (2020).

9 Chau, T. N. *et al.* SARS-associated viral hepatitis caused by a novel coronavirus: report of three cases. *Hepatology* **39**, 302-310, doi:10.1002/hep.20111 (2004).

10 Ding, Y. *et al.* The clinical pathology of severe acute respiratory syndrome (SARS): a report from China. *J Pathol* **200**, 282-289, doi:10.1002/path.1440 (2003).

11 Li, S. *et al.* Clinical and pathological investigation of patients with severe COVID-19. *JCI Insight* **5**, doi:10.1172/jci.insight.138070 (2020).

12 To, K. K. *et al.* Lessons learned one year after SARS-CoV-2 emergence leading to COVID-19 pandemic. *Emerg Microbes Infect*, 1-89, doi:10.1080/22221751.2021.1898291 (2021).

13 Li, X., Sridhar, S. & Chan, J. F. The Coronavirus Disease 2019 pandemic: how does it spread and how do we stop it? *Curr Opin HIV AIDS* **15**, 328-335, doi:10.1097/COH.0000000000000650 (2020).

14 Yeung, M. L. *et al.* MERS coronavirus induces apoptosis in kidney and lung by upregulating Smad7 and FGF2. *Nat Microbiol* **1**, 16004, doi:10.1038/nmicrobiol.2016.4 (2016).

15 Chan, J. F. *et al.* Simulation of the Clinical and Pathological Manifestations of Coronavirus Disease 2019 (COVID-19) in a Golden Syrian Hamster Model: Implications for Disease Pathogenesis and Transmissibility. *Clin Infect Dis* **71**, 2428-2446, doi:10.1093/cid/ciaa325 (2020).

16 McIlwain, D. R., Berger, T. & Mak, T. W. Caspase functions in cell death and disease. *Cold Spring Harb Perspect Biol* **5**, a008656, doi:10.1101/cshperspect.a008656 (2013).

17 Li, K. *et al.* Mouse-adapted MERS coronavirus causes lethal lung disease in human DPP4 knockin mice. *Proc Natl Acad Sci U S A* **114**, E3119-E3128, doi:10.1073/pnas.1619109114 (2017).

18 Lee, A. C. *et al.* Oral SARS-CoV-2 Inoculation Establishes Subclinical Respiratory Infection with Virus Shedding in Golden Syrian Hamsters. *Cell Rep Med* **1**, 100121, doi:10.1016/j.xcrm.2020.100121 (2020).

19 Parrish, A. B., Freel, C. D. & Kornbluth, S. Cellular mechanisms controlling caspase activation and function. *Cold Spring Harb Perspect Biol* **5**, doi:10.1101/cshperspect.a008672 (2013).

20 Wang, X. J., Cao, Q., Zhang, Y. & Su, X. D. Activation and regulation of caspase-6 and its role in neurodegenerative diseases. *Annu Rev Pharmacol Toxicol* **55**, 553-572, doi:10.1146/annurev-pharmtox-010814-124414 (2015).

21 Desmyter, J., Melnick, J. L. & Rawls, W. E. Defectiveness of interferon production and of rubella virus interference in a line of African green monkey kidney cells (Vero). *J Virol* **2**, 955-961, doi:10.1128/JVI.2.10.955-961.1968 (1968).

22 Osada, N. *et al.* The genome landscape of the african green monkey kidney-derived vero cell line. *DNA Res* **21**, 673-683, doi:10.1093/dnares/dsu029 (2014).

23 Lui, P. Y. *et al.* Middle East respiratory syndrome coronavirus M protein suppresses type I interferon expression through the inhibition of TBK1-dependent phosphorylation of IRF3. *Emerg Microbes Infect* **5**, e39, doi:10.1038/emi.2016.33 (2016).

24 Siu, K. L. *et al.* Middle east respiratory syndrome coronavirus 4a protein is a double-stranded RNA-binding protein that suppresses PACT-induced activation of RIG-I and MDA5 in the innate antiviral response. *J Virol* **88**, 4866-4876, doi:10.1128/JVI.03649-13 (2014).

25 Yang, Y. *et al.* The structural and accessory proteins M, ORF 4a, ORF 4b, and ORF 5 of Middle East respiratory syndrome coronavirus (MERS-CoV) are potent interferon antagonists. *Protein Cell* **4**, 951-961, doi:10.1007/s13238-013-3096-8 (2013).

26 Talanian, R. V. *et al.* Substrate specificities of caspase family proteases. *J Biol Chem* **272**, 9677-9682, doi:10.1074/jbc.272.15.9677 (1997).

27 McBride, R., van Zyl, M. & Fielding, B. C. The coronavirus nucleocapsid is a multifunctional protein. *Viruses* **6**, 2991-3018, doi:10.3390/v6082991 (2014).

28 Hoffmann, M. *et al.* SARS-CoV-2 Cell Entry Depends on ACE2 and TMPRSS2 and Is Blocked by a Clinically Proven Protease Inhibitor. *Cell* **181**, 271-280 e278, doi:10.1016/j.cell.2020.02.052 (2020).

29 Chu, H. *et al.* Host and viral determinants for efficient SARS-CoV-2 infection of the human lung. *Nat Commun* **12**, 134, doi:10.1038/s41467-020-20457-w (2021).

30 Wurzer, W. J. *et al.* Caspase 3 activation is essential for efficient influenza virus propagation. *EMBO J* **22**, 2717-2728, doi:10.1093/emboj/cdg279 (2003).

31 Muhlbauer, D. *et al.* Influenza virus-induced caspase-dependent enlargement of nuclear pores promotes nuclear export of viral ribonucleoprotein complexes. *J Virol* **89**, 6009-6021, doi:10.1128/JVI.03531-14 (2015).

32 Graham, R. K., Ehrnhoefer, D. E. & Hayden, M. R. Caspase-6 and neurodegeneration. *Trends Neurosci* **34**, 646-656, doi:10.1016/j.tins.2011.09.001 (2011).

33 Eleouet, J. F. *et al.* The viral nucleocapsid protein of transmissible gastroenteritis coronavirus (TGEV) is cleaved by caspase-6 and -7 during TGEV-induced apoptosis. *J Virol* **74**, 3975-3983, doi:10.1128/jvi.74.9.3975-3983.2000 (2000).

34 Oh, C., Kim, Y. & Chang, K. O. Caspase-mediated cleavage of nucleocapsid protein of a protease-independent porcine epidemic diarrhea virus strain. *Virus Res* **285**, 198026, doi:10.1016/j.virusres.2020.198026 (2020).

35 Chu, H. *et al.* Comparative tropism, replication kinetics, and cell damage profiling of SARS-CoV-2 and SARS-CoV with implications for clinical manifestations, transmissibility, and laboratory studies of COVID-19: an observational study. *Lancet Microbe* **1**, e14-e23, doi:10.1016/S2666-5247(20)30004-5 (2020).

36 Chan, J. F. *et al.* Differential cell line susceptibility to the emerging novel human betacoronavirus 2c EMC/2012: implications for disease pathogenesis and clinical manifestation. *J Infect Dis* **207**, 1743-1752, doi:10.1093/infdis/jit123 (2013).

37 Chu, H. *et al.* Productive replication of Middle East respiratory syndrome coronavirus in monocyte-derived dendritic cells modulates innate immune response. *Virology* **454-455**, 197-205, doi:10.1016/j.virol.2014.02.018 (2014).

38 Chu, H. *et al.* Tetherin/BST-2 is essential for the formation of the intracellular virus-containing compartment in HIV-infected macrophages. *Cell Host Microbe* **12**, 360-372, doi:10.1016/j.chom.2012.07.011 (2012).

39 Yuan, S. *et al.* SREBP-dependent lipidomic reprogramming as a broad-spectrum antiviral target. *Nat Commun* **10**, 120, doi:10.1038/s41467-018-08015-x (2019).

40 Yuan, S. *et al.* Viruses harness YxxO motif to interact with host AP2M1 for replication: A vulnerable broad-spectrum antiviral target. *Sci Adv* **6**, eaba7910, doi:10.1126/sciadv.aba7910 (2020).

41 Chu, H. *et al.* Comparative Replication and Immune Activation Profiles of SARS-CoV-2 and SARS-CoV in Human Lungs: An Ex Vivo Study With Implications for the Pathogenesis of COVID-19. *Clin Infect Dis* **71**, 1400-1409, doi:10.1093/cid/ciaa410 (2020).

42 Zhou, J. *et al.* Active replication of Middle East respiratory syndrome coronavirus and aberrant induction of inflammatory cytokines and chemokines in human macrophages: implications for pathogenesis. *J Infect Dis* **209**, 1331-1342, doi:10.1093/infdis/jit504 (2014).

43 Zhou, J. *et al.* Infection of bat and human intestinal organoids by SARS-CoV-2. *Nat Med* **26**, 1077-1083, doi:10.1038/s41591-020-0912-6 (2020).

44 Chan, J. F. *et al.* Surgical Mask Partition Reduces the Risk of Noncontact Transmission in a Golden Syrian Hamster Model for Coronavirus Disease 2019 (COVID-19). *Clin Infect Dis* **71**, 2139-2149, doi:10.1093/cid/ciaa644 (2020).

45 Yuan, S. *et al.* Metallodrug ranitidine bismuth citrate suppresses SARS-CoV-2 replication and relieves virus-associated pneumonia in Syrian hamsters. *Nat Microbiol* **5**, 1439-1448, doi:10.1038/s41564-020-00802-x (2020).

46 Chan, C. M. *et al.* Carcinoembryonic Antigen-Related Cell Adhesion Molecule 5 Is an Important Surface Attachment Factor That Facilitates Entry of Middle East Respiratory Syndrome Coronavirus. *J Virol* **90**, 9114-9127, doi:10.1128/JVI.01133-16 (2016).

47 Chu, H. *et al.* SARS-CoV-2 Induces a More Robust Innate Immune Response and Replicates Less Efficiently Than SARS-CoV in the Human Intestines: An Ex Vivo Study With Implications on Pathogenesis of COVID-19. *Cell Mol Gastroenterol Hepatol* **11**, 771-781, doi:10.1016/j.jcmgh.2020.09.017 (2021).

48 Chu, H. *et al.* Middle East respiratory syndrome coronavirus and bat coronavirus HKU9 both can utilize GRP78 for attachment onto host cells. *J Biol Chem* **293**, 11709-11726, doi:10.1074/jbc.RA118.001897 (2018).

49 The UniProt, C. UniProt: a worldwide hub of protein knowledge. *Nucleic Acids Research* **47**, D506-D515, doi:10.1093/nar/gky1049 (2018).

50 Edgar, R. C. MUSCLE: multiple sequence alignment with high accuracy and high throughput. *Nucleic Acids Research* **32**, 1792-1797, doi:10.1093/nar/gkh340 (2004).

51 Berman, H. M. *et al.* The Protein Data Bank. *Nucleic acids research* **28**, 235-242, doi:10.1093/nar/28.1.235 (2000).

Figures and Figures Legends

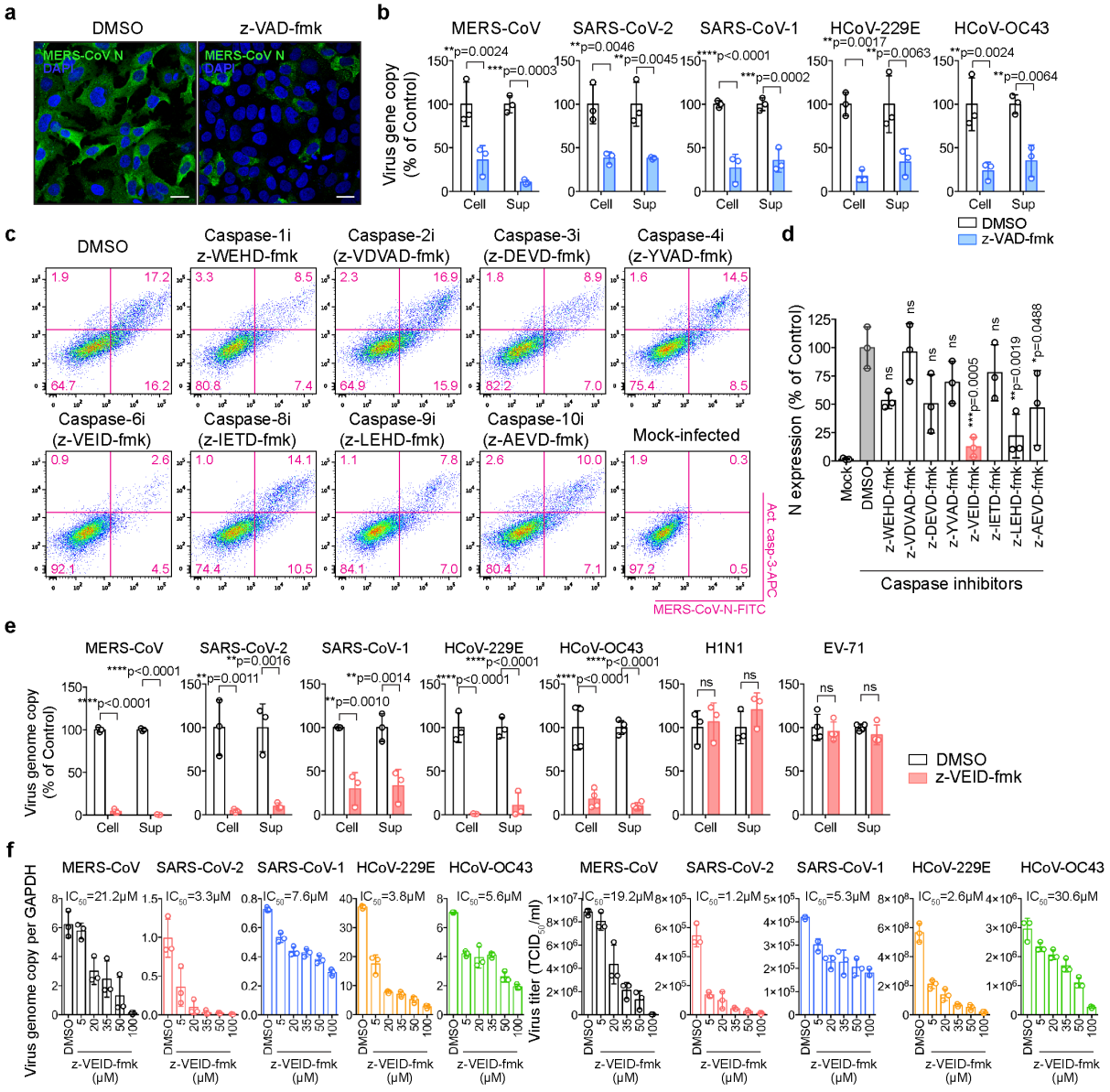

Figure 1. Caspase-6 inhibition limits coronavirus replication. a MERS-CoV-infected Huh7 cells were treated with 100μM z-VAD-fmk or DMSO. Cells were fixed at 24 hpi and immunolabeled with an in-house guinea pig immune serum against MERS-CoV N. **b** Replication of human-pathogenic coronaviruses treated with 100μM z-VAD-fmk or DMSO. Samples were harvested at 24 hpi and viral gene expression was quantified with RT-qPCR (n=3). **c-d** Flow cytometry of MERS-CoV-infected BEAS2B cells treated with 75μM specific caspase inhibitors. Cells were fixed at 24 hpi and labelled with the MERS-CoV N immune

serum and an active caspase-3 antibody (n=3). **e** Virus replication of MERS-CoV (BEAS2B), SARS-CoV-2 (Calu3), SARS-CoV-1 (Huh7), HCoV-229E (Huh7), HCoV-OC43 (BSC-1), H1N1 (A549), and EV-71 (RD) with or without 100μM z-VEID-fmk. Virus gene copy was quantified with RT-qPCR. **f** The half-maximal inhibitory concentrations (IC_{50s}) of z-VEID-fmk on the replication of MERS-CoV (HFL), SARS-CoV-2 (Calu3), SARS-CoV-1 (Huh7), HCoV-229E (Huh7) and HCoV-OC43 (BSC-1) in cell lysate and supernatant samples were determined with RT-qPCR and $TCID_{50}$ assays, respectively (n=4 for HCoV-OC43 and EV-71, n=3 for other viruses). Data represented mean and standard deviations from the indicated number of biological repeats. Statistical significance between groups was determined with one way-ANOVA (**d**) or two way-ANOVA (**b** and **e**). * represented $p < 0.05$, ** represented $p < 0.01$, *** represented $p < 0.001$, **** represented $p < 0.0001$. ns = not significant. Bars in (**a**) represented 20μm.

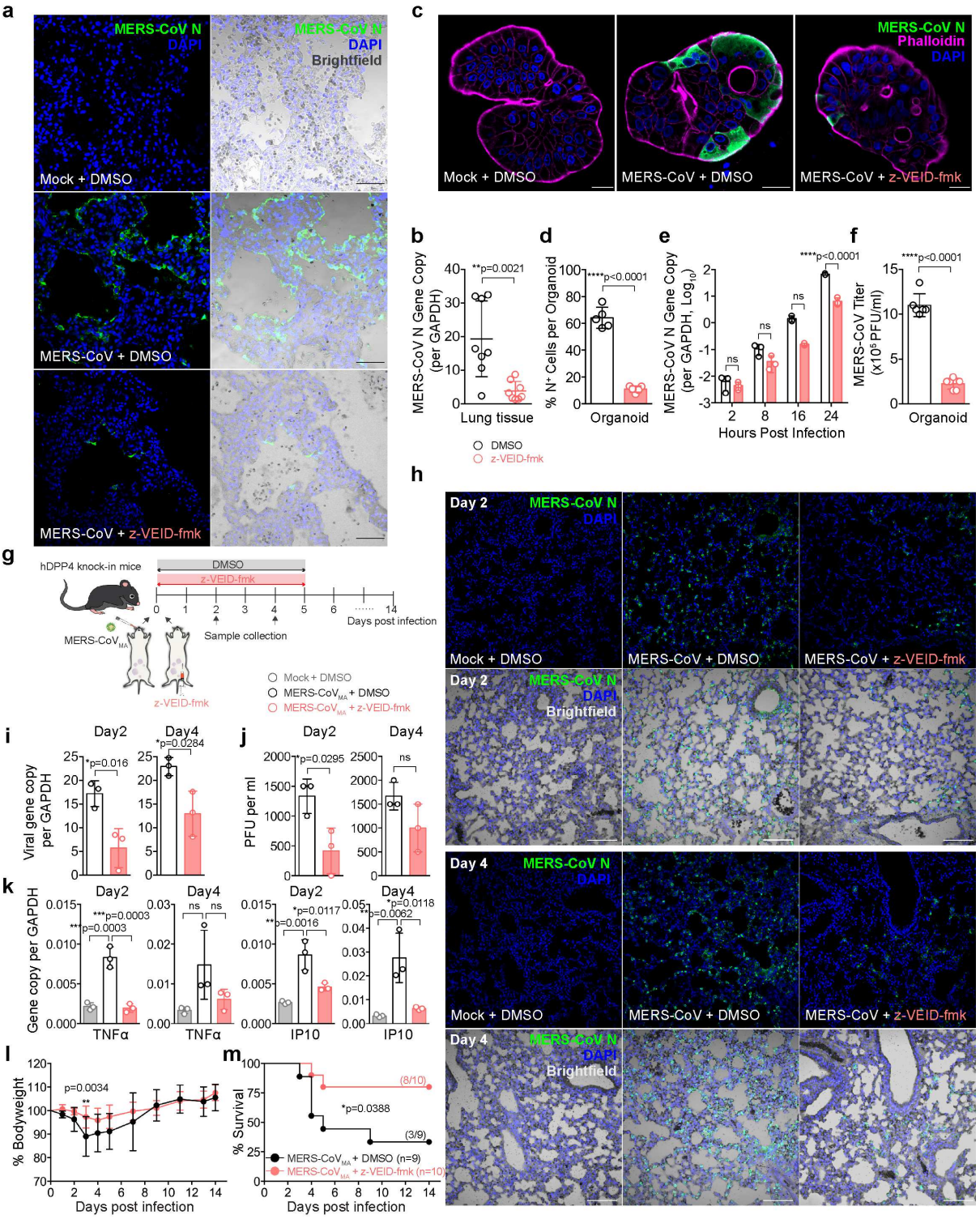

Figure 2. Caspase-6 inhibition attenuates MERS-CoV replication in human lung tissues, human intestinal organoids, and improves the survival of hDPP4 KI mice. a-b *Ex vivo* human lung tissues were infected with MERS-CoV and treated with z-VEID-fmk. The tissues and supernatants were harvested at 24 hpi for immunostaining with an in-house guinea pig

immune serum against MERS-CoV N (**a**) and RT-qPCR (n=8) (**b**). **c-f** Human intestinal organoids were infected with MERS-CoV and treated with z-VEID-fmk. Organoids were fixed at 24 hpi for immunostaining for N protein expression (**c**). The percentage of infected cells per organoids was calculated from counting the number of infected cells and uninfected cells per organoid (n=5) (**d**). N gene expression at the indicated time points was quantified with RT-qPCR (n=3) (**e**). Infectious titer was determined with plaque assays (n=6) (**f**). **g** hDPP4 KI mice were intranasally inoculated with $2.5x10^3$PFU MERS-CoV_{MA} followed by intraperitoneal administration of 12.5mg/kg/day z-VEID-fmk or DMSO for 6 days or until sample harvest. **h** A subset of mice were harvested at day 2 and day 4 post infection. Mouse lungs were immunolabelled to detect MERS-CoV N expression. **i** Viral gene expression in mouse lungs were quantified with RT-qPCR (n=3). **j** Infectious titer was determined with plaque assays (n=3). **k** Expression of pro-inflammatory cytokines and chemokines were quantified with RT-qPCR. **l-m** Body weight and survival of the infected mice were monitored for 14 days. Data represented mean and standard deviations from the indicated number of biological repeats. Statistical significance between groups was determined with one way-ANOVA (**k**), two way-ANOVA (**e**), Student's t-test (**b, d, f, i, j, and l**), or Log-rank (Mantel-Cox) test (**m**). * represented $p < 0.05$, ** represented $p < 0.01$, *** represented $p < 0.001$, **** represented $p < 0.0001$. ns = not significant. Bars in (**a, c, and h**) represented 50μm, 20μm, and 100μm, respectively.

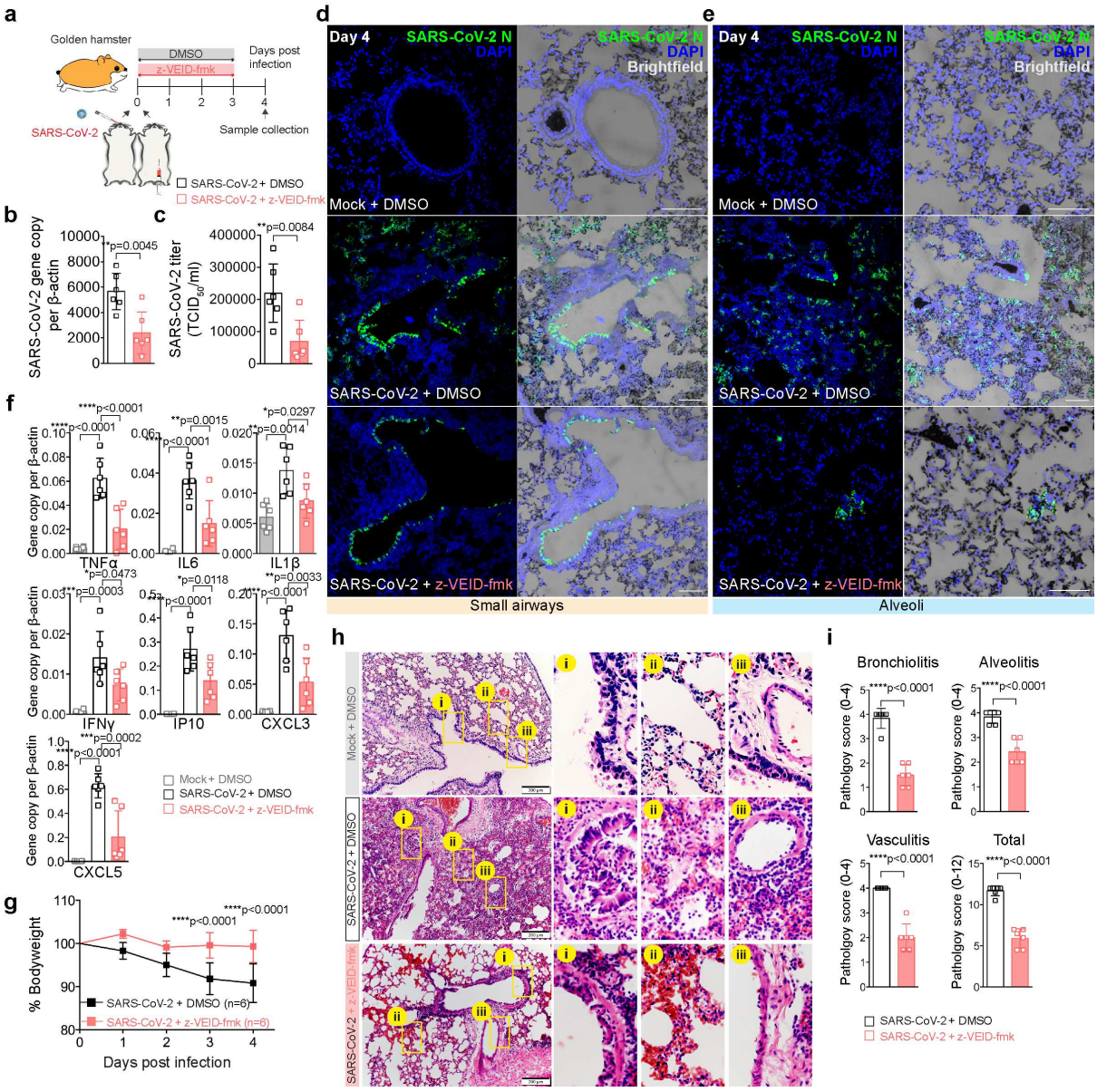

Figure 3. Caspase-6 inhibition ameliorates lung pathology and improves the body weight of SARS-CoV-2-infected golden Syrian hamsters. **a** Golden Syrian hamsters were intranasally inoculated with $3x10^3$PFU SARS-CoV-2 followed by intraperitoneal administration of 12.5mg/kg/day z-VEID-fmk or DMSO for 4 days. **b-c** Hamsters were sacrificed at day 4 post infection, viral gene copy and infectious titer of hamster lungs were quantified with RT-qPCR and $TCID_{50}$ assays, respectively (n=6). **d-e** Viral N protein expression in the small airways and alveoli of infected hamster lungs with or without z-VEID-fmk treatment was revealed with immunofluorescence staining with the in-house rabbit immune serum against SARS-CoV-2 N. **f** Expression of pro-inflammatory cytokines and chemokines was quantified with RT-qPCR

(n=6). **g** Body weight change of SARS-CoV-2-infected hamsters with z-VEID-fmk or mock treatment was documented from day 0 to day 4 post infection. **h** Representative images of haematoxylin and eosin (H&E) stained hamster lungs. (Top panels) mock-infected hamster lung sections showed normal histology, boxed areas were magnified showing (i) intact bronchiolar epithelium lining, (ii) thin alveolar wall and clear air sac, and (iii) a normal structure of pulmonary blood vessel section. (Middle panels) In SARS-CoV-2-infected hamsters, lung tissues showed diffuse inflammatory infiltration and exudation with disappearing air-exchange structures. Boxed areas were magnified to demonstrate the characteristic histopathological changes (i) peribronchiolar infiltration and bronchiolar epithelium desquamation, (ii) alveolar infiltration and haemorrhage with alveolar space filled with infiltrated immune cell and protein-rich exudate, (iii) pulmonary blood vessel showed immune cells infiltration in the vessel wall, endothelium, and perivascular connective tissue. (Bottom panels) The hamster lung pathology was markedly improved with z-VEID-fmk treatment. Magnified images demonstrated (i) milder degree of immune cell infiltration in bronchiolar epithelium and peribronchiolar tissue, (ii) thickened alveolar wall with red blood cells but alveolar space showed no immune cell infiltration nor exudation, (iii) pulmonary vessel wall showed a few immune cells attached to the endothelium. **i** Quantitative scores for the lung histopathological changes of SARS-CoV-2-infected hamsters with or without z-VEID-fmk treatment. Three categories of characteristic histopathological changes including bronchiolitis, alveolitis and vasculitis were examined and scored. (n=6 and two-three lung lobes were examined from each hamster). Data represented mean and standard deviations from the indicated number of biological repeats. Statistical significance between groups was determined with one way-ANOVA (**f**) or Student's t-test (**b, c, g, and i**). * represented $p < 0.05$, ** represented $p < 0.01$, *** represented $p < 0.001$, **** represented $p < 0.0001$. ns = not significant. Bars in (**d and e)** represented 100μm.

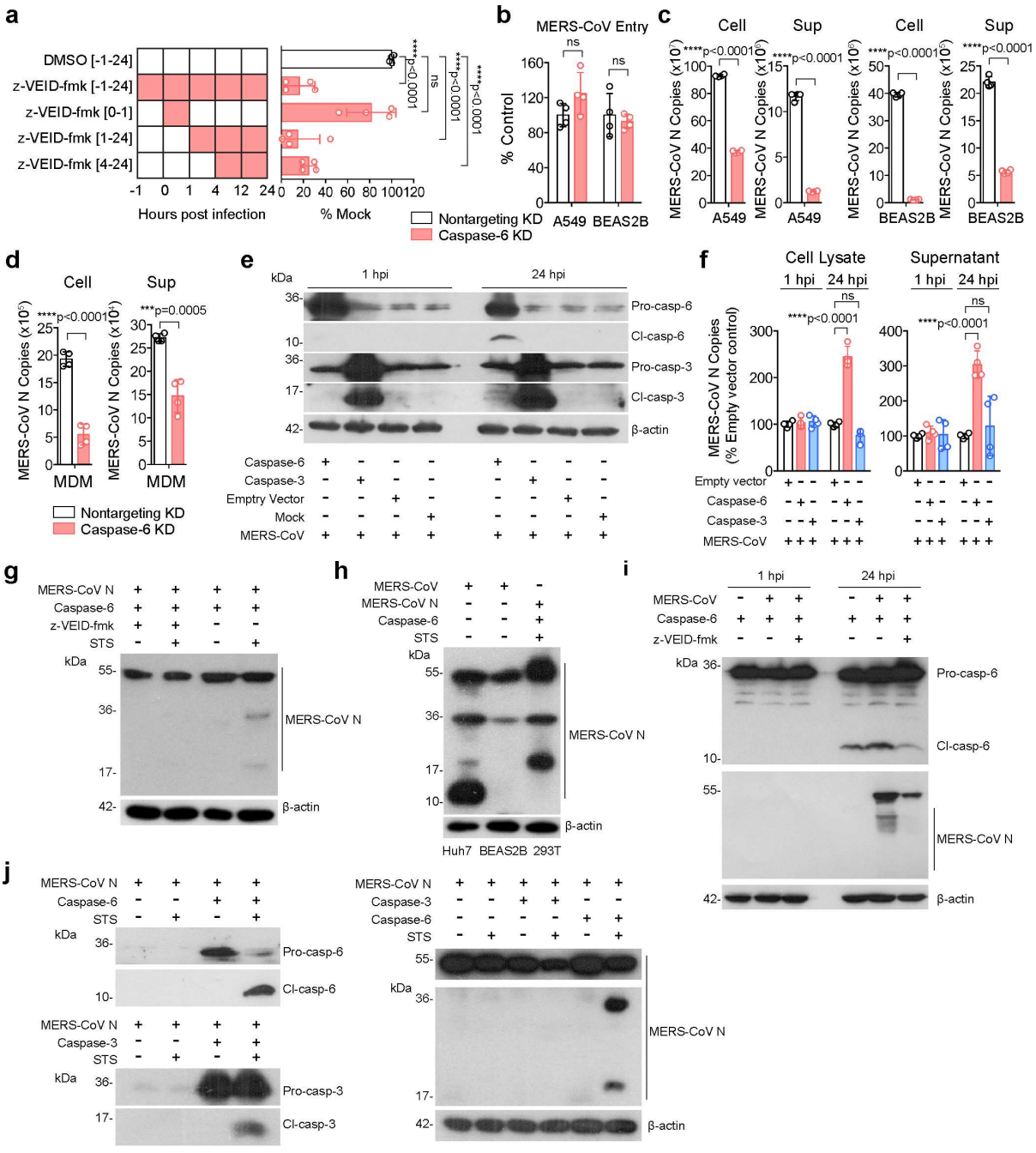

Figure 4. Caspase-6 modulates MERS-CoV replication at a post entry step and cleaves MERS-CoV N protein. a MERS-CoV-infected BEAS2B cells were incubated with z-VEID-fmk in a time of addition assay. Virus gene copy in the supernatant was determined with RT-qPCR at 24hpi (n=4). **b-c** Caspase-6 stable knockdown A549 and BEAS2B cells were infected with MERS-CoV at 0.1MOI. (**b**) Cell lysates were harvested at 1 hpi to quantify virus entry with RT-qPCR (n=4). (**c**) Virus replication at 24 hpi were quantified with RT-qPCR (n=4). **d** MDMs were treated with caspase-6 or nontargeting siRNA and infected with MERS-CoV. Virus gene

copy was quantified at 24 hpi (n=4). **e-f** Caspase-6- or caspase-3-overexpressed 293T cells were infected with MERS-CoV at 1MOI. Virus replication was quantified at 1 and 24 hpi with RT-qPCR (n=4). **g** MERS-CoV N and caspase-6 were co-expressed in 293T cells with or without 100μM z-VEID-fmk. Cells were harvested for Western blot at 24 hours post transfection. 1μM staurosporine (STS) was added as an apoptosis trigger at 6 hours before sample harvest. **h** N cleavage in cell lysates from MERS-CoV-infected Huh7 and BEAS2B cells was compared to the N cleavage in cell lysates from MERS-CoV N and caspase-6 co-transfected 293T cells. **i** N cleavage in MERS-CoV-infected cells with or without z-VEID-fmk. **j** Comparison of MERS-CoV N cleavage in caspase-6-overexpressed and caspase-3-overexpressed cells. Data represented mean and standard deviations from the indicated number of biological repeats. Statistical significance between groups was determined with one way-ANOVA (**a**), two-way ANOVA (**b and f**), or Student's t-test (**c and d**). * represented $p < 0.05$, ** represented $p < 0.01$, *** represented $p < 0.001$, **** represented $p < 0.0001$. ns = not significant.

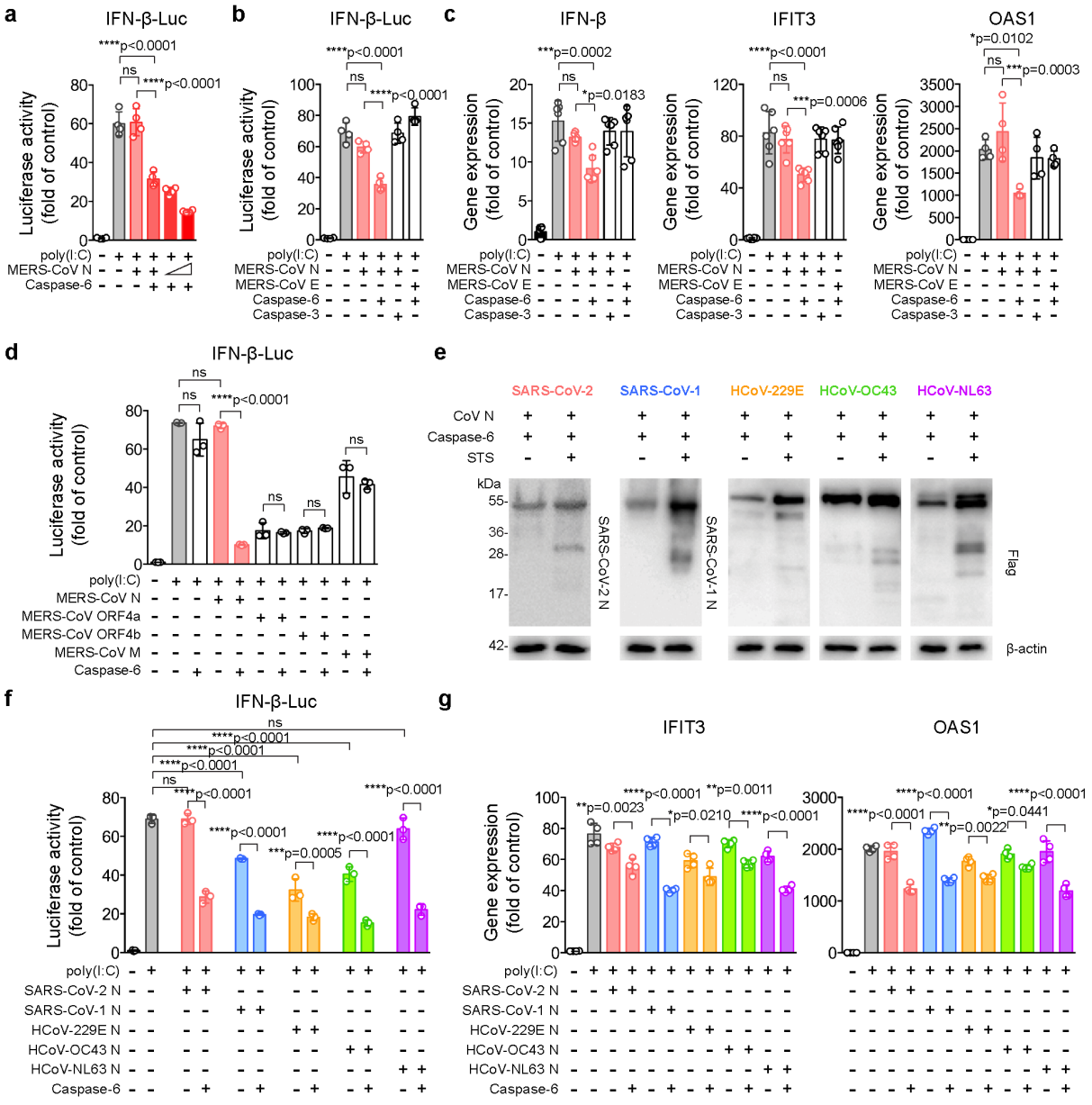

Figure 5. Caspase-6-mediated coronavirus N cleavage interferes with IFN signalling.

a-b 293T cells were transfected with an IFN-β-Luc reporter plasmid, expression constructs of MERS-CoV N or E and caspase-6 or caspase-3, with or without poly(I:C). Cells were incubated for 24 hours before harvesting for dual-luciferase reporter assays (n=4). **c** 293T cells were transfected with the same set of plasmids. Gene expression of IFN-β, IFIT3, and OAS1 was quantified with RT-qPCR (n=6 for IFN-β and IFIT1, n=4 for OAS1). **d** 293T cells were transfected with an IFN-β-Luc reporter plasmid, expression constructs of caspase-6 and MERS-CoV N, ORF4a, ORF4b, or M, with or without poly(I:C). Cells were incubated for 24 hours

before harvesting for dual-luciferase reporter assays (n=3). **e** N protein of the indicated coronaviruses were co-expressed with caspase-6. N cleavage was detected with Western blots. **f** 293T cells were transfected with an IFN-β-Luc reporter plasmid, expression constructs of caspase-6 and coronavirus N, with or without poly(I:C). Cells were incubated for 24 hours before harvesting for dual-luciferase reporter assays (n=3). **g** 293T cells were transfected with the same set of plasmids. Gene expression of IFIT3 and OAS1 was quantified with RT-qPCR (n=4). Data represented mean and standard deviations from the indicated number of biological repeats. Statistical significance between groups was determined with one way-ANOVA (**a-f and h-i**). * represented $p < 0.05$, ** represented $p < 0.01$, *** represented $p < 0.001$, **** represented $p < 0.0001$. ns = not significant.

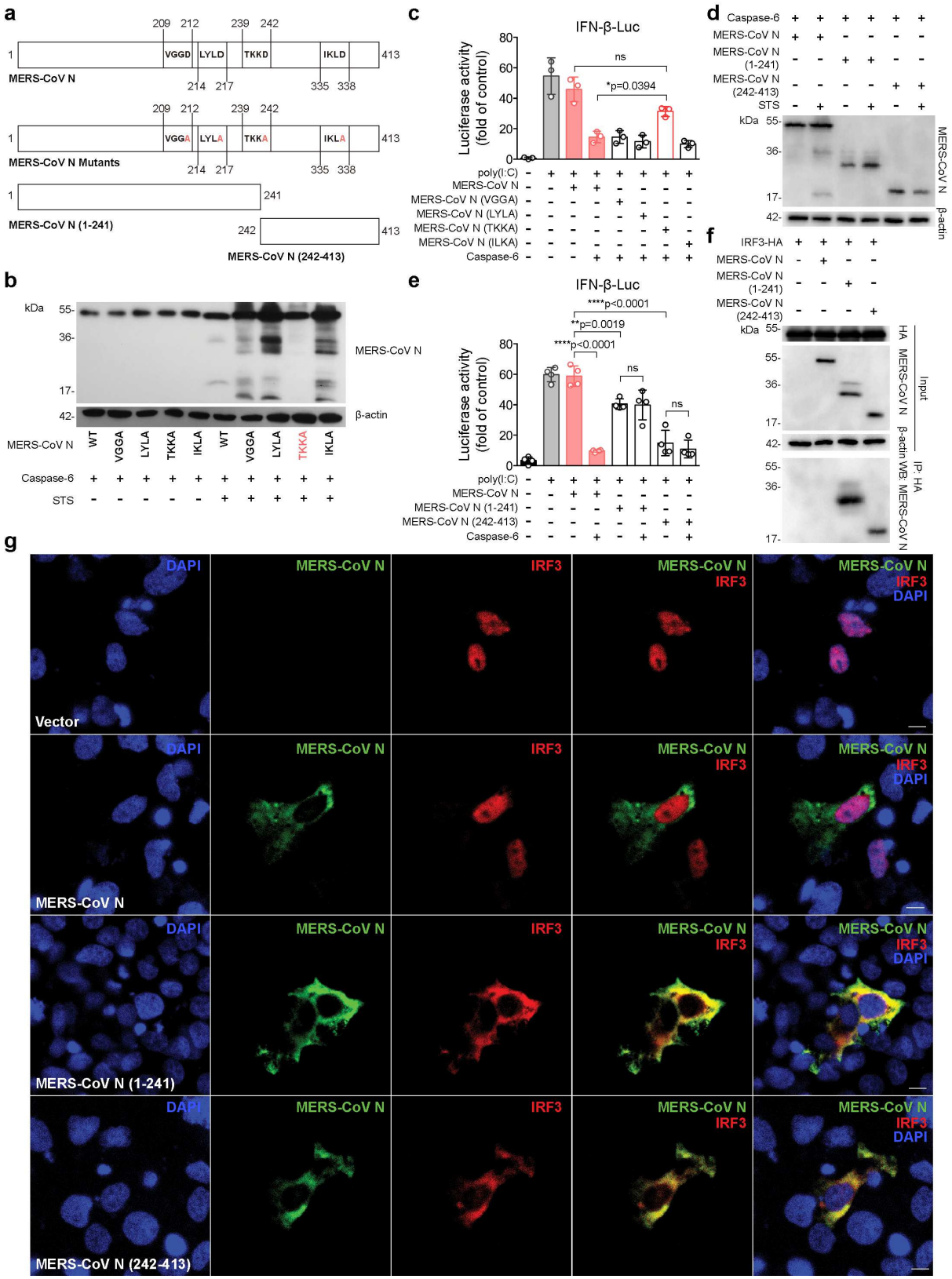

Figure 6. Caspase-6-mediated MERS-CoV N cleavage generates N fragments that block IRF3 translocation to the cell nucleus. a Schematic of N mutants. **b** Caspase-6-mediated cleavage of N mutants was evaluated with Western blots. **c** 293T cells were transfected with an

IFN-β-Luc reporter plasmid, expression constructs of caspase-6 and MERS-CoV N or N mutants, with or without poly(I:C). Cells were incubated for 24 hours before harvesting for dual-luciferase reporter assays (n=3). **d** Caspase-6-mediated cleavage of N, N(1-241), and N(242-413) was evaluated with Western blots. **e** 293T cells were transfected with an IFN-β-Luc reporter plasmid, expression constructs of caspase-6 and MERS-CoV N, N(1-241), or N(242-413), with or without poly(I:C). Cells were incubated for 24 hours before harvesting for dual-luciferase reporter assays (n=4). **f** Interaction between IRF3 and N, N(1-241), or N(242-413) was evaluated with co-immunoprecipitation assays using IRF3 as the bait protein. **g** 293T cells were transfected with expression constructs of IRF3, N, N(1-241), or N(242-413), and poly(I:C). Cells were fixed at 24 hours post transfection. Localization of N was detected with an in-house guinea pig anti-N immune serum and IRF3 was detected with a rabbit anti-HA antibody. Cell nuclei were identified with the DAPI stain. Data represented mean and standard deviations from the indicated number of biological repeats. Statistical significance between groups was determined with one way-ANOVA (**c and e**). * represented $p < 0.05$, ** represented $p < 0.01$, *** represented $p < 0.001$, **** represented $p < 0.0001$. ns = not significant. Bars in (**g**) represented 10μm.

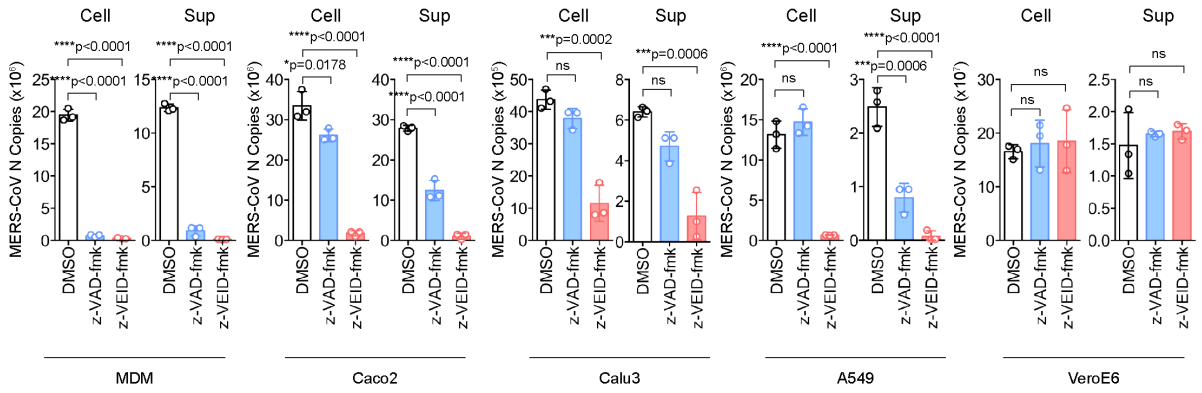

Extended Data Figure 1. Caspase-6 inhibition reduces MERS-CoV replication in different cell types. MDM, Caco2, Calu3, A549, and VeroE6 cells were infected with MERS-CoV at 1MOI and were treated with z-VEID-fmk, z-VAD-fmk, or DMSO. Cell lysate and supernatant samples were harvested at 24hpi. Virus gene copy was quantified with RT-qPCR (n=3). Data represented mean and standard deviations from the indicated number of biological repeats. Statistical significance between groups was determined with one way-ANOVA. * represented $p < 0.05$, ** represented $p < 0.01$, *** represented $p < 0.001$, **** represented $p < 0.0001$. ns = not significant.

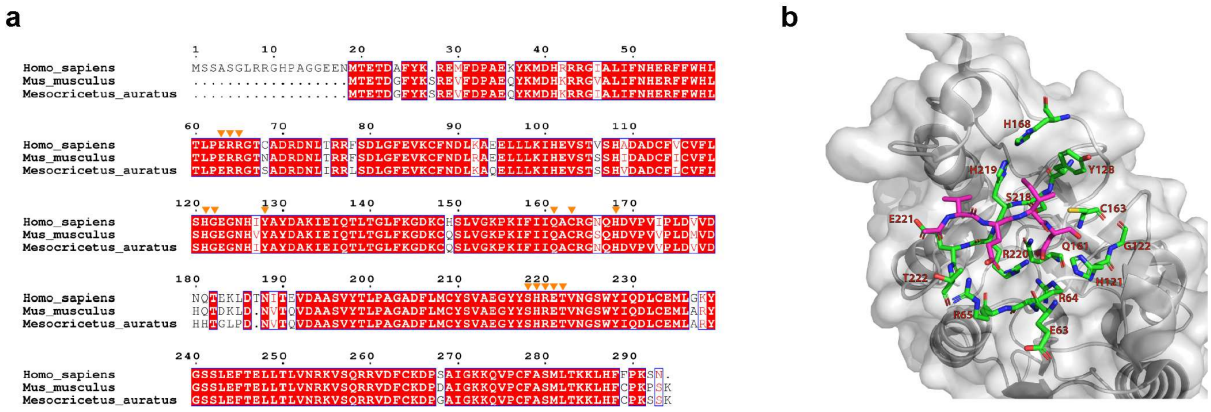

Extended Data Figure 2. The z-VEID-fmk binding pocket is conserved in human, mouse, and golden Syrian hamster caspase-6. a Multiple sequence alignment of human, mouse and golden Syrian hamster caspase-6 full-length sequences. The indices were labelled according to human caspase-6. VEID binding sites on caspase-6 were indicated with orange triangles. **b** VEID binding mode represented in 3D structure. Binding sites on caspase-6 and VEID were shown in green and magenta sticks, respectively. The binding site residues were labelled in red.

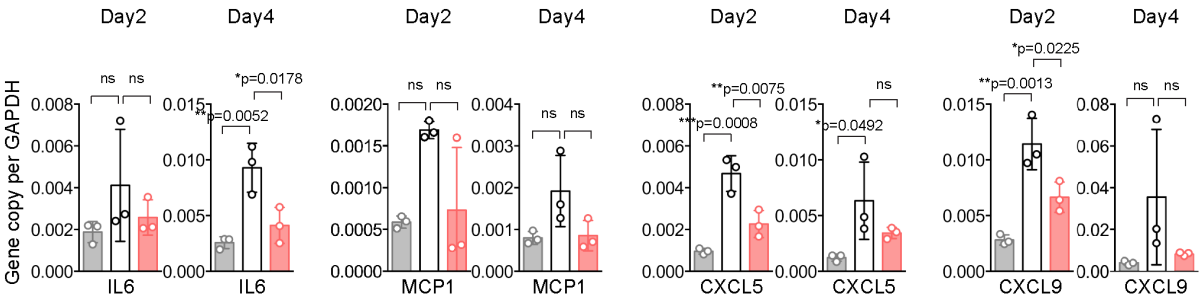

Extended Data Figure 3. Caspase-6 inhibition reduces the expression of pro-inflammatory cytokines and chemokines in the lungs of hDPP4 KI mice. hDPP4 KI mice were intranasally inoculated with $2.5x10^3$PFU MERS-CoV_{MA} followed by intraperitoneal administration of 12.5mg/kg/day z-VEID-fmk or DMSO for 6 days or until sample harvest. Mouse lungs were harvested at day 2 and day 4 post infection. Expression of pro-inflammatory cytokines and chemokines were quantified with RT-qPCR. Data represented mean and standard deviations from the indicated number of biological repeats. Statistical significance between groups was determined with one way-ANOVA. * represented $p < 0.05$, ** represented $p < 0.01$, *** represented $p < 0.001$. ns = not significant

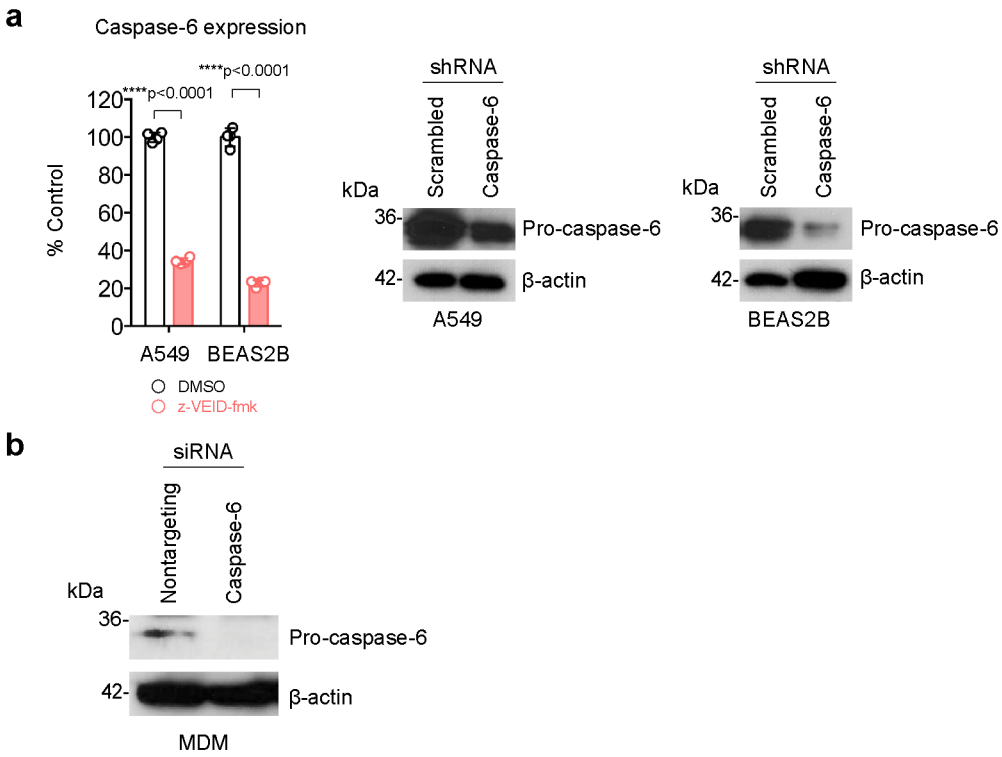

741

742 **Extended Data Figure 4. Caspase-6 knockdown efficiency in cell lines and MDMs.**

743 **a** Caspase-6 RNA (n=3) and protein expression from caspase-6 stable knockdown A549 and

744 BEAS2B cells. **b** Caspase-6 protein expression from caspase-6 siRNA transfected MDMs. Data

745 represented mean and standard deviations from the indicated number of biological repeats.

746 Statistical significance between groups was determined with two way-ANOVA. ****

747 represented $p < 0.0001$.

748

749

750

751

752

753

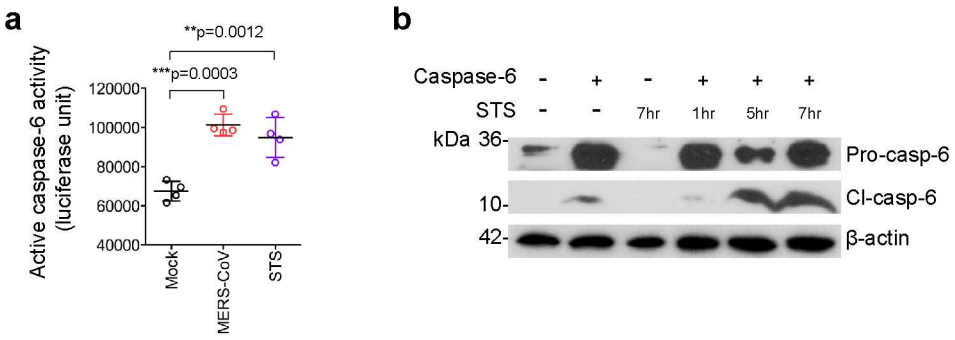

754

755 **Extended Data Figure 5. Caspase-6 is activated by apoptosis and can undergo**
756 **autoactivation. a** Caspase-6 is activated by apoptosis triggered by MERS-CoV infection or
757 staurosporine (STS) stimulation. Huh7 cells were infected with MERS-CoV at 1MOI for 12
758 hours. In parallel, Huh7 cells were stimulated with STS at 1μM for 6 hours. Caspase-6 activity
759 in the cell lysate was determined with the caspase-Glo-6 assay kit (n=4). **b** Autoactivation and
760 STS-mediated activation of caspase-6 were demonstrated with Western blots. Data represented
761 mean and standard deviations from the indicated number of biological repeats. Statistical
762 significance between groups was determined with two way-ANOVA. ** represented $p < 0.01$
763 and *** represented $p < 0.001$.

764

765

766

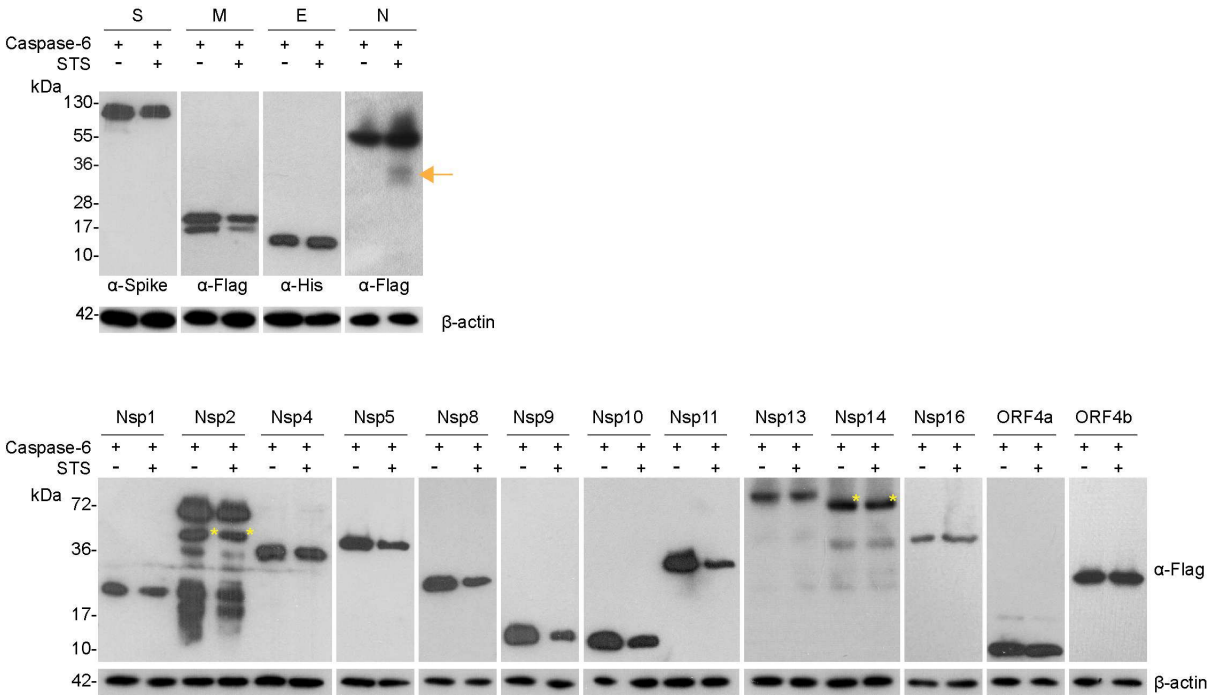

Extended Data Figure 6. Caspase-6 cleaves MERS-CoV N but not other MERS-CoV proteins. Caspase-6 and expression constructs for MERS-CoV proteins were transfected in 293T cells. Caspase-6-mediated cleavage was detected with Western blots. Asterisks at Nsp2 and Nsp14 indicated the predicted protein sizes according to the number of amino acid residues. Caspase-6-specific cleavage product was only observed when N was co-expressed with caspase-6 (arrow).

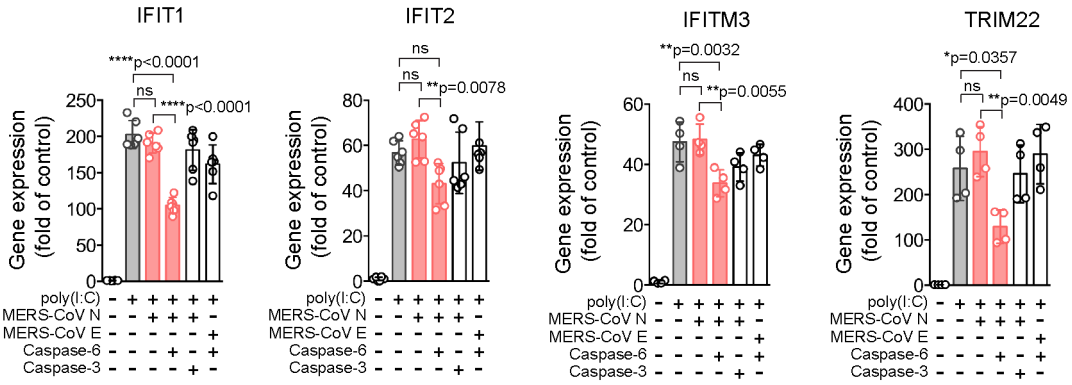

Extended Data Figure 7. Caspase-6-mediated N cleavage reduces ISG expression. 293T cells were transfected with an IFN-β-Luc reporter plasmid, expression constructs of MERS-CoV N or E and caspase-6 or caspase-3, with or without poly(I:C). Gene expression of IFIT1, IFIT2, IFITM3, and TRIM22 was quantified with RT-qPCR (n=6 for IFIT1 and IFIT2, n=4 for IFITM3 and TRIM22). Data represented mean and standard deviations from the indicated number of biological repeats. Statistical significance between groups was determined with one way-ANOVA. * represented $p < 0.05$, ** represented $p < 0.01$, *** represented $p < 0.001$, **** represented $p < 0.0001$. ns = not significant.

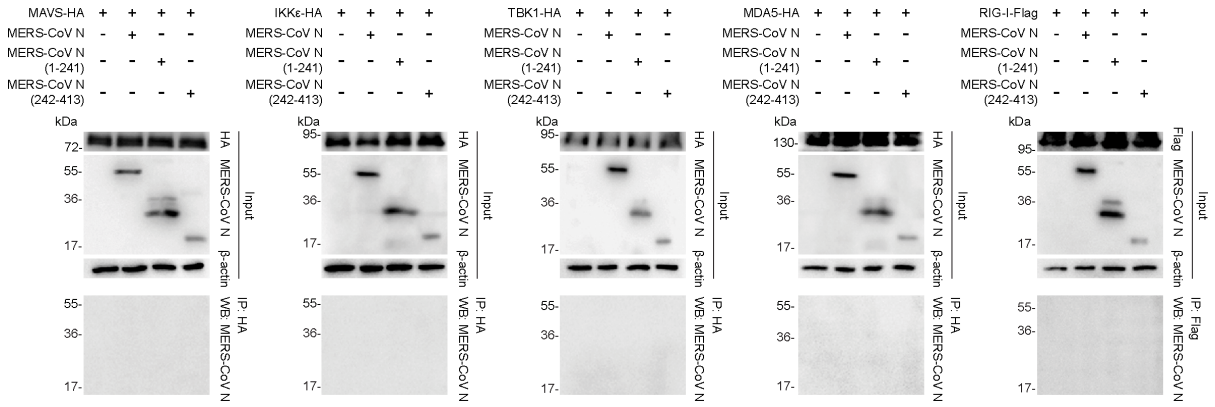

799

800 **Extended Data Figure 8. Caspase-6-cleaved N fragments do not bind MAVS, IKKε,**

801 **TBK1, MDA5, or RIG-I.** Interaction between MAVS, IKKε, TBK1, MDA5, and RIG-I with

802 N, N(1-241), or N(242-413) was evaluated with co-immunoprecipitation assays.

803

804

805

806

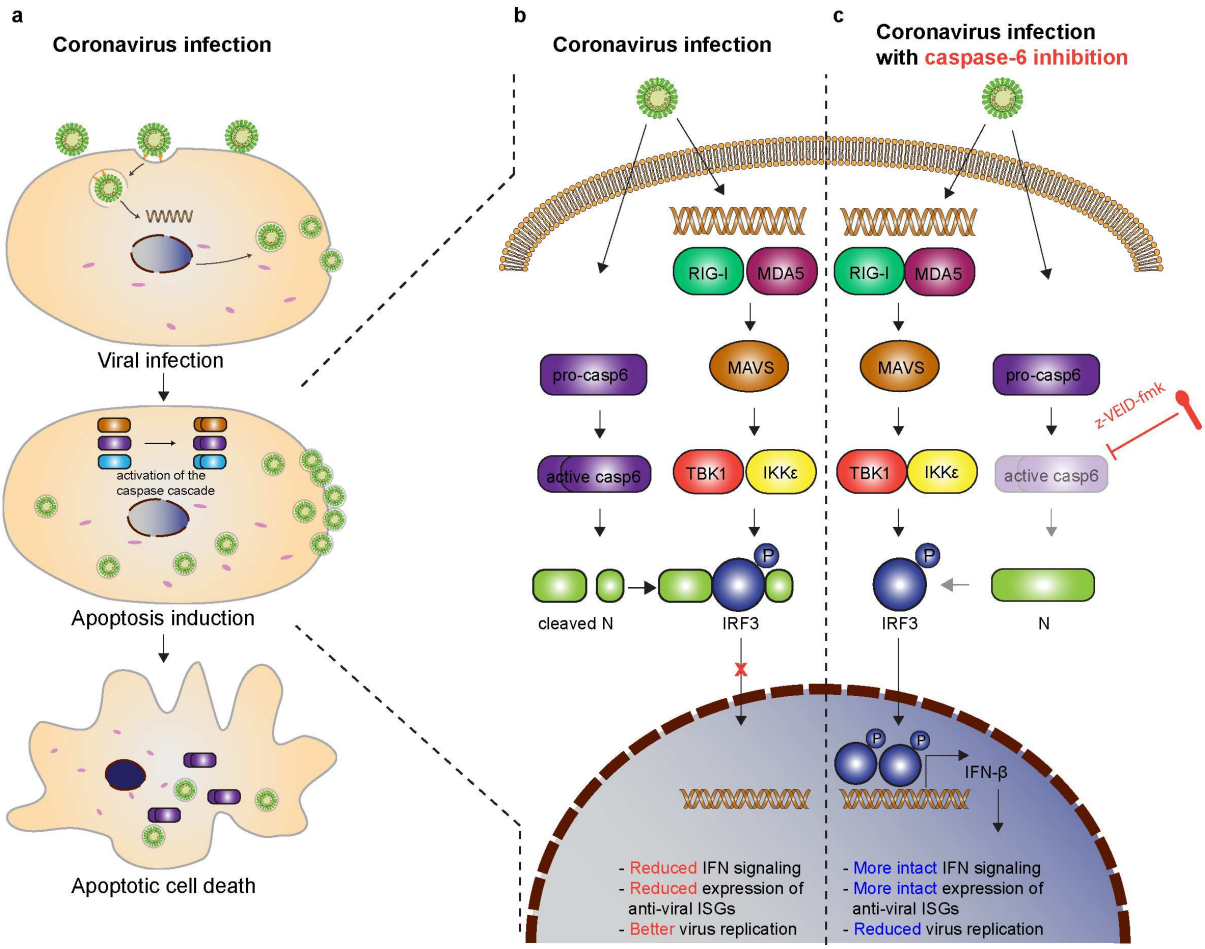

807

808 **Extended Data Figure 9. Current model of how caspase-6 facilitates coronavirus**
809 **replication using MERS-CoV as an example. a** Upon coronavirus infection, the host initiates
810 apoptosis to eliminate infected cells, aiming to terminate virus propagation. The triggered
811 apoptosis cascade leads to activation of executor caspases (caspase-3, -6, -7). **b** MERS-CoV
812 exploits caspase-6 to cleave its N protein, generating N fragments that bind to IRF3, attenuating
813 the activation of IFN signalling, thus benefits virus replication. **c** In the presence of caspase-6
814 inhibition, N is not cleaved and IFN signalling is more intact, resulting in restricted virus
815 replication.

816

817

818

819

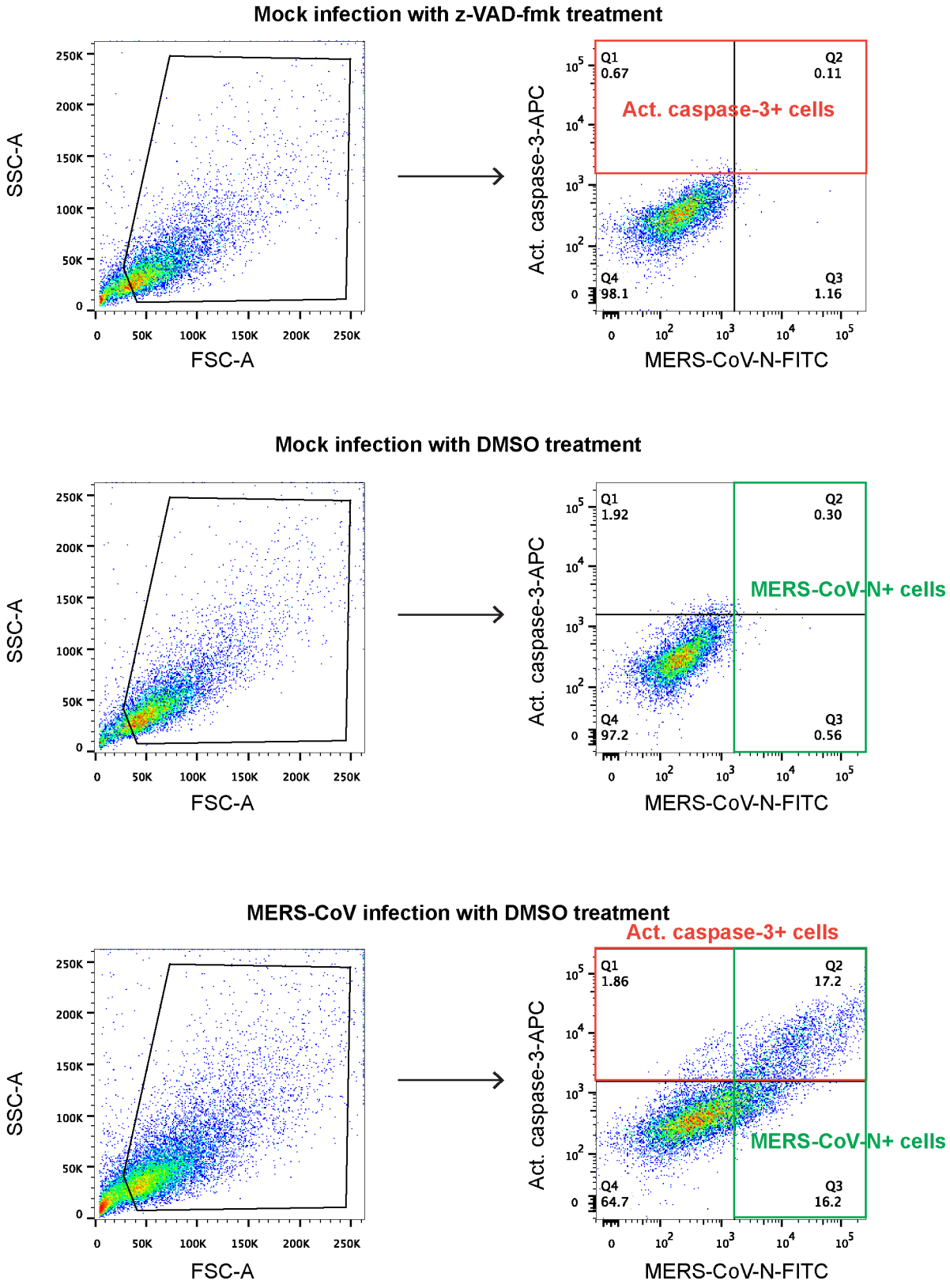

Extended Data Figure 10. Gating Strategy for the flow cytometry experiment in Figure 1.

The BEAS2B cell population was gated with SSC-A vs FSC-A. Most cells with the exception of the cell debris at the lower left corner were gated. A mock-infected sample treated with the

apoptosis inhibitor, z-VAD-fmk, was used as the gating control for active caspase-3-positive cells. A mock-infected sample treated with DMSO was used as the gating control for MERS-CoV-N-positive cells.

Materials and methods

Cell lines

A549, BSC-1, Caco2, Huh7, VeroE6, and 293T cells were maintained in Dulbecco's Modified Eagle medium (DMEM) supplemented with 10% heat-inactivated fetal bovine serum (FBS), 100unit/ml penicillin, and 100μg/ml streptomycin[35,36]. BEAS2B and Calu3 cells were maintained in DMEM/F12 supplemented with 10% heat-inactivated FBS, 100unit/ml penicillin and 100μg/ml streptomycin. HFL (primary human embryonic lung fibroblast) were maintained in Minimum Essential Medium (MEM) supplemented with 10%heat-inactivated FBS, 100unit/ml penicillin and 100μg/ml streptomycin. Human primary monocytes were obtained from human peripheral blood mononuclear cells (PBMCs) taken from healthy donors, collected from Hong Kong Red Cross Blood Transfusion Service according to a protocol approved by the Institutional Review Board of the University of Hong Kong[37]. Primary human monocyte-derived macrophages (MDMs) were differentiated from monocytes in Roswell Park Memorial Institute (RPMI)-1640 media supplemented with 10% heat-inactivated FBS, 100unit/ml penicillin, 100μg/ml streptomycin, 2mM glutamine, 1% sodium pyruvate, 1% non-essential amino acids, and 10ng/ml recombinant human granulocyte macrophage colony-stimulating factor (GM-CSF) (R&D Systems) as we previously described[38].

Viruses

The MERS-CoV (EMC/2012) strain of MERS-CoV was provided by Dr. Ron Fouchier (Erasmus Medical Center). The mouse-adapted MERS-CoV (MERS-CoV$_{MA}$) was a gift from

Dr. Paul McCray (University of Iowa, IA, USA). SARS-CoV-2 HKU-001a was isolated from a nasopharyngeal aspirate specimen taken from a laboratory-confirmed COVID-19 patient in Hong Kong[35]. SARS-CoV-1 GZ50, HCoV-229E, HCoV-OC43, enterovirus A71, and influenza A virus strain A/Hong Kong/415742/2009(H1N1)pdm09 were archived clinical isolates at Department of Microbiology, HKU[39,40]. All infectious experiments involving MERS-CoV, SARS-CoV-2 and SARS-CoV-1 followed the approved standard operating procedures of the Biosafety Level 3 facility at the Department of Microbiology, HKU.

Chemical modulators

The pan-caspase inhibitor, z-VAD-fmk, was obtained from Invivogen. The caspase-1-to-caspase-10 inhibitor sampler kit was purchased from R&D Systems. The caspase-6 inhibitors, z-VEID-fmk, used for *in vitro* and *in vivo* experiments, were obtained from R&D Systems and APExBIO, respectively. The apoptosis enhancer, staurosporine, was obtained from Sigma.

Antibodies

MERS-CoV N, MERS-CoV Spike, SARS-CoV-1 N and SARS-CoV-2 N were detected with specific in-house immune serum. Primary antibodies including rabbit anti-caspase-3, rabbit anti-caspase-6, rabbit anti-HA, mouse anti-Flag, mouse anti-His, and mouse anti-β-actin were from Abcam. Secondary antibodies including goat anti-mouse horseradish peroxidase (HRP), goat anti-rabbit HRP and goat anti-guinea pig HRP from Thermo Fisher Scientific were used for Western blots. Alexa Fluor 488 goat anti-guinea pig, Alexa Fluor 488 goat anti-rabbit and Alexa Fluor 568 goat anti-rabbit from Thermo Fisher Scientific were used for immunohistochemistry staining.

***Ex vivo* human lung tissues**

Ex vivo human lung tissues were processed and infected with MERS-CoV we previously described[41,42]. Human lung tissues for *ex vivo* studies were retrieved from patients underwent surgical operations at the Queen Mary Hospital, Hong Kong. All donors gave written consent as approved by the Institutional Review Board of the University of Hong Kong/Hospital Authority Hong Kong West Cluster. Normal nonmalignant lung tissue fragments in excess for clinical diagnosis were used. The freshly obtained lung tissues were processed into small rectangular pieces and were rinsed with the primary tissue culture medium, which contained the advanced DMEM/F12 medium supplemented with 2mM HEPES (Gibco), 1x GlutaMAX (Gibco), 100unit/ml penicillin, 100μg/ml streptomycin, 20μg/ml vancomysin, 20μg/ml ciprofloxacin, 50μg/ml amikacin, and 50μg/ml nystatin. The specimens were infected with MERS-CoV at a titer of $1x10^8$PFU/ml. After 2 h, the inoculum was removed and the specimens were washed thoroughly with the primary tissue culture medium. The infected tissues were then incubated with primary tissue culture medium supplemented with 100μM caspase-6 inhibitor z-VEID-fmk dissolved in DMSO or DMSO only. Tissues were harvested at 24 hpi with either 10% neutral-buffered formalin for immunofluorescence staining or with RL buffer for RT-qPCR analysis.

Human intestinal organoids

Human Intestinal organoids were established using biopsied human intestinal tissues from patients who underwent surgical operations at the Queen Mary Hospital, Hong Kong[43]. All donors had written consent as approved by the Institutional Review Board of the University of Hong Kong/Hospital Authority Hong Kong West Cluster. Human intestinal organoids were maintained in expansion medium and induced differentiation by incubating with differentiation media for 5 days as we previously described[43]. Differentiated intestinal organoids were sheared mechanically and inoculated with MERS-CoV at 1MOI for 2 h. After the inoculum was removed, the intestinal organoids were rinsed with PBS and embedded in Matrigel and

maintained in differentiation medium containing 100μM z-VEID-fmk. At the indicated time points after inoculation, intestinal organoids were harvested for the quantification of intracellular viral load and immunofluorescence staining, whereas the cell-free Matrigel and culture medium were combined for viral titration of extracellular virions using standard plaque assays.

Human DPP4 mouse model

The hDPP4 knockin (KI) mice were kindly provided by Dr. Paul McCray (University of Iowa, IA, USA)[17]. The use of animals has complied with all relevant ethical regulations and was approved by the Committee on the Use of Live Animals in Teaching and Research of The University of Hong Kong. On the day of infection, hDPP4 KI mice were intranasally (i.n.) inoculated with $2.5x10^3$PFU mouse-adapted MERS-CoV ($MERS\text{-}CoV_{MA}$) pre-diluted in 20μl DMEM, followed by intraperitoneal (i.p.) injection with 12.5mg/kg/day z-VEID-fmk or DMSO diluted in 200μl 0.3% methylcellulose/0.1% tween-80/PBS for 6 days or until sample harvest. The health status and body weight of the mice were monitored for 14 days on a daily basis or until the animal is sacrificed or euthanized because of reaching the humane endpoint of the experiment. Mice were sacrificed at the designated time points and lung tissue from mice of both treatment and control groups were harvested for immunofluorescence staining, RT-qPCR, and plaque assay analysis.

Golden Syrian hamster model

Infection of golden Syrian hamsters was performed as we described previously[15]. Golden Syrian hamsters aged 6-8 weeks old were obtained from the Chinese University of Hong Kong Laboratory Animal Service Centre through the HKU Centre for Comparative Medicine Research (CCMR). The use of animals has complied with all relevant ethical regulations and was approved by the Committee on the Use of Live Animals in Teaching and Research of

924 The University of Hong Kong. On the day of infection, each hamster was intranasally
925 inoculated with $3x10^3$PFU SARS-CoV-2 pre-diluted in 50µl DMEM under intraperitoneal
926 ketamine (100mg/kg) and xylazine (10mg/kg) anesthesia. Infected hamsters were treated with
927 12.5mg/kg/day z-VEID-fmk or DMSO diluted in 600µl 0.3% methylcellulose/0.1% tween-
928 80/PBS for 4 days. The health status and body weight of the hamsters were monitored on a
929 daily basis or until the animal is sacrificed or euthanized because of reaching the humane
930 endpoint of the experiment. Hamsters were sacrificed at day 4 post infection and lung tissues
931 were harvested for immunofluorescence staining, histopathology examination, RT-qPCR, and
932 $TCID_{50}$ assay analysis[44,45].
933
934 **RNA extraction and quantitative RT-PCR**
935 Cells were lysed in RL buffer and extracted with the MiniBEST Universal RNA Extraction Kit
936 (TaKaRa). Viral RNA in the supernatant was extracted with the MiniBEST Viral RNA/DNA
937 Extraction Kit (TaKaRa). Reverse transcription (RT) and quantitative polymerase chain reaction
938 (qPCR) were performed with Transcriptor First Strand cDNA Synthesis Kit and LightCycler
939 480 master mix from Roche. All primer and probe sequences were provided in Extended Data
940 Table 2.
941
942 **Plaque assays and $TCID_{50}$ assays**
943 Infectious titers of MERS-CoV and SARS-CoV-2 were determined with standard plaque
944 assays[35]. In brief, VeroE6 cells were seeded in 24-well plates 1 day before the experiment. The
945 harvested supernatant samples were serially diluted and inoculated to the cells for 2 h at 37°C.
946 After inoculation, the cells were washed with PBS 3 times, and covered with 2% agarose/PBS
947 mixed with 2× DMEM/2%FBS at 1:1 ratio. The cells were fixed after incubation at 37°C for 72
948 h. Fixed samples were stained with 0.5% crystal violet in 25% ethanol/distilled water for 10 min

for plaque visualization. In some experiments, infectious titers of coronaviruses were determined with standard $TCID_{50}$ assays. In brief, VeroE6 cells were seeded in 96-well plates 1 day before the experiment. The harvested supernatant samples were serially diluted and inoculated to the cells for 2 h at 37°C. After inoculation, the cells were washed with PBS 3 times and incubation at 37°C. After 72 hpi, virus titer was calculated using the Muench and Reed method.

siRNA and shRNA knockdown

On-Targetplus caspase-6 siRNA was obtained from Dharmacon. Transfection of siRNA on MDMs was performed using Lipofectamine RNAiMAX (Thermo Fisher Scientific) as we previously described[46]. In brief, the cells were transfected with 50nM caspase-6 siRNA for two consecutive days. At 24 hours after the second siRNA transfection, the cells were harvested in RIPA buffer for Western blot analysis. In parallel, siRNA-transfected cells were challenged with MERS-CoV at 1MOI for 1 h at 37°C. Following the inoculation, the cells were washed with PBS and incubated for 24 h. The virus copy number at 24 hpi was determined with RT-qPCR. pLKO.1 lentiviral caspase-6 shRNA plasmid was obtained from Dharmacon. Transfection of caspase-6 shRNA plasmid, psPAX2 packaging plasmid and pMD2.G envelope plasmid on 293T cells was performed using Lipofectamine 3000 (Thermo Fisher Scientific) following manufacturer's manual. In brief, 293T cells in 10cm dishes were transfected with 6 μg caspase-6 shRNA plasmid, 4.5μg packaging plasmid, and 1.5μg envelope plasmid in FBS-supplemented DMEM medium, followed by aspirating supernatant at 6 h post transfection and replacing with FBS-free medium. On the next day, the supernatant containing caspase-6 shRNA lentivirus particles was harvested and was used to transduce A549 and BEAS2B cells. A549 and BEAS2B caspase-6 stable knockdowns cells were selected by 0.5μg/mL and 0.7μg/mL puromycin, respectively. The selected cells were challenged with MERS-CoV at 0.1MOI for 1 h at 37°C. The virus copy number at 1 and 24 hpi was determined with RT-qPCR.

Caspase-6 activity assay

Huh7 cells were infected with MERS-CoV at 1MOI for 12 h. In parallel, Huh7 cells were stimulated with STS at 1μM for 6 h. Caspase-6 activity in the cell lysate was determined with the caspase-Glo-6 assay kit (Promega). The luminescence signal of caspase-6 activity was measured following manufacturer's manual with a multilabel plate reader Victor X3 (Perkin-Elmer).

Immunofluorescence and histology

Immunofluorescence staining was performed as we previously described with slight modifications[47]. Briefly, infected human and animal lung tissues were fixed overnight in 10% formalin. The fixed samples were then embedded in paraffin with a TP1020 Leica semi-enclosed benchtop tissue processor and sectioned at 5μm. Tissue sections were fished and dried to fix on Thermo Fisher Scientific Superfrost Plus slides at 37°C overnight. Antigen retrieval was performed by heating the slides in antigen unmasking solution (Vector Laboratories) for 90 seconds. MERS-CoV and SARS-CoV-2 were detected with an in-house guinea pig anti-MERS-CoV-N immune serum and an in-house rabbit anti-SARS-CoV-2-N immune serum, respectively. Cell nuclei were labeled with the DAPI nucleic acid stain (Thermo Fisher Scientific). Alexa Fluor secondary antibodies were obtained from Thermo Fisher Scientific. Mounting was performed with the Diamond Prolong Antifade Mountant from Thermo Fisher Scientific. Images were captured with an Olympus BX53 fluorescence microscope (Olympus Life Science, Tokyo, Japan) or a Carl Zeiss LSM 780 confocal microscope in the faculty core facility of HKU. For H&E staining, hamster lung tissue sections were stained with Gill's hematoxylin and eosin Y (Thermo Fisher Scientific). H&E stained hamster lung tissue sections were blinded for the identities of experimental settings and examined by a trained

999 histopathologist. Lung pathology was graded on a scale of 0 (normal) to 4 (most severe)
1000 according to a grading system we previously described[18].
1001
1002 **Western blot**
1003 Cells were lysed by RIPA buffer (Thermo Fisher Scientific) with protease inhibitor (Roche,
1004 Basel, Switzerland). Proteins were separated with SDS-PAGE and transferred to PVDF
1005 membranes (Thermo Fisher Scientific). Specific primary antibodies were incubated with the
1006 blocked membranes at 4°C overnight, followed by horseradish peroxidase (HRP) conjugated
1007 secondary antibodies (Thermo Fisher Scientific) for 1 h at room temperature. The signal was
1008 developed by Immobilon Crescendo Western HRP Substrate (Merck Millipore, MA, USA) and
1009 detected using automatic x-ray film processor (Advansta) or an Alliance Q9 Advanced imager
1010 (Uvitec, Cambridge, UK).
1011
1012 **Flow cytometry**
1013 BEAS2B cells were infected with MERS-CoV at 1MOI. At 24 hpi, the cells were detached with
1014 10mM EDTA in PBS, fixed in 4% paraformaldehyde, followed by immunolabeling with an in-
1015 house guinea pig anti-MERS-CoV-N immune serum and a rabbit anti-active caspase-3 antibody
1016 (BD). Flow cytometry was performed using a BD FACSCanto II flow cytometer (BD) and data
1017 was analyzed using FlowJo X 10.0.7 (BD) as we previously described[48]. The gating strategy was
1018 demonstrated in **Extended Data Figure 10**.
1019
1020 **IFN-β-luciferase reporter assays**
1021 IFN-β-luciferase reporter assays were performed as we previously described[23,24]. In brief, 500ng
1022 IFN-β-luciferase reporter plasmid, 10ng transfection efficiency control plasmid (pNL1.1.TK,
1023 Promega), 1μg coronavirus N plasmids, 3μg caspase-6 expression plasmid, together with or

without 5μg Poly(I:C) were co-transfected into 293T cells for 24 h. On the next day, the cells were harvested for luciferase measurement with the dual-luciferase reporter assay system kit (Promega) according to the manufacturer's protocol using a multilabel plate reader Victor X3 (Perkin-Elmer).

Alignment of human, mouse, and hamster caspase-6

Caspase-6 protein sequences of homo sapiens (Uniprot ID: P55212), mus musculus (Uniprot ID: O08738) and mesocricetus auratus (Uniprot ID: A0A1U7QNN7) were downloaded from UniProt[49]. Multiple sequence alignment was performed with MUSCLE[50]. The crystal structure of caspase-6 and VEID complex was retrieved from the Protein Data Bank (PDB code: 3OD5)[51]. Caspase-6 residues within 4Å of VEID were defined as the binding sites and visualized with Pymol.

Prediction of potential caspase-6 cleavage sites

The protein sequence of MERS-CoV N (NC_019843) was used for caspase-6 cleavage site analysis. Potential caspase-6 cleavage motifs on MERS-CoV N was determined based on published substrate specificity of caspase-6[26]. The amino acid pattern "[TVILENYF]..D" was search against the N sequence, where "." represented any amino acid.

Statistical analysis

Data on figures represented means and standard deviations. Statistical comparison between different groups was performed by one-way ANOVA, two-way ANOVA, Student's t-test, or Log-rank (Mantel-Cox) test using GraphPad Prism 6. Differences were considered statistically significant when $p < 0.05$.

Figures

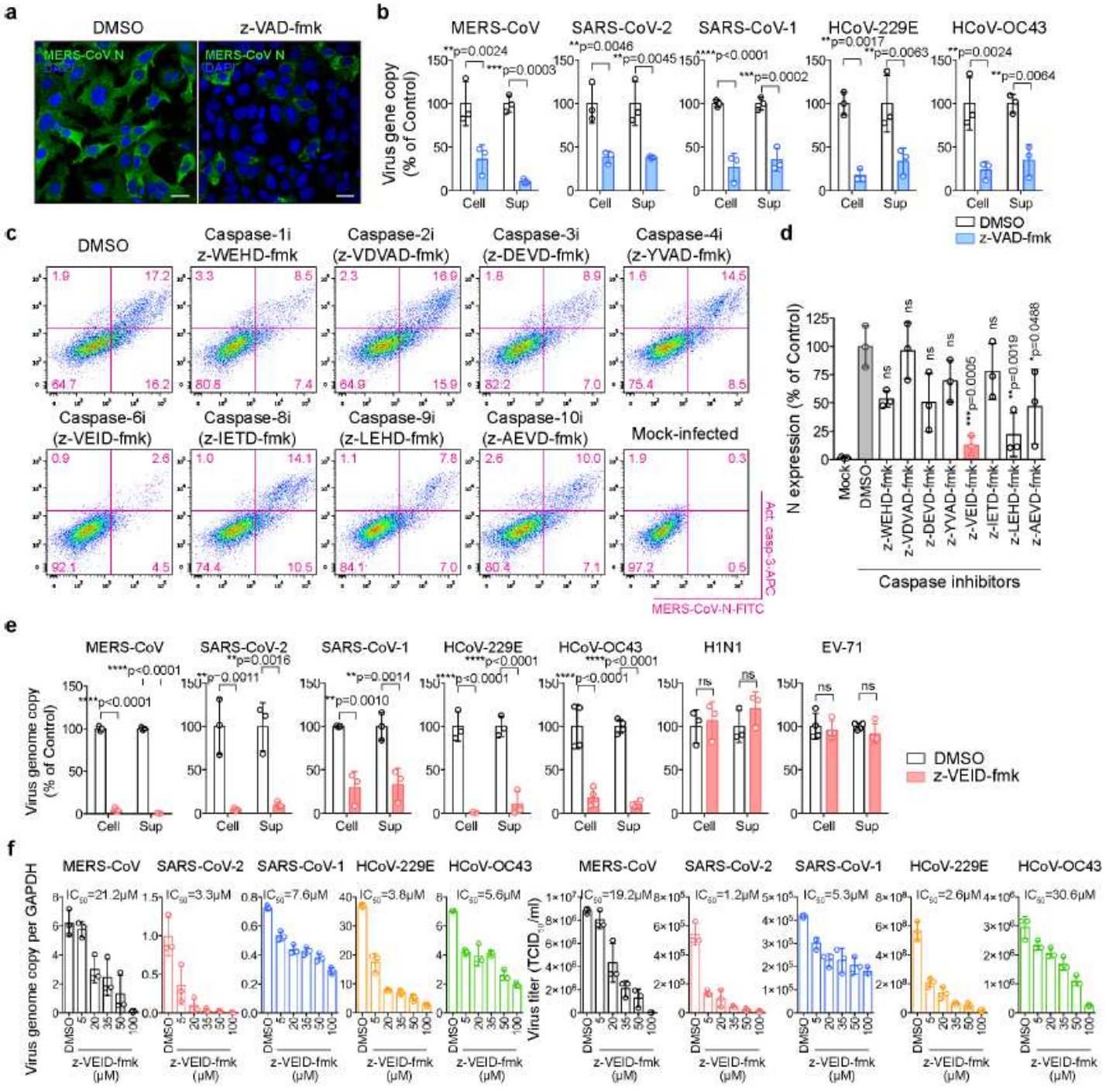

Figure 1

Caspase-6 inhibition limits coronavirus replication. a MERS-CoV-infected Huh7 cells were treated with 100μM z-VAD-fmk or DMSO. Cells were fixed at 24 hpi and immunolabeled with an in-house guinea pig immune serum against MERS-CoV N. b Replication of human-pathogenic coronaviruses treated with 100μM z-VAD-fmk or DMSO. Samples were harvested at 24 hpi and viral gene expression was quantified with RT-qPCR (n=3). c-d Flow cytometry of MERS-CoV-infected BEAS2B cells treated with 75μM specific

caspase inhibitors. Cells were fixed at 24 hpi and labelled with the MERS-CoV N immune serum and an active caspase-3 antibody (n=3). e Virus replication of MERS-CoV (BEAS2B), SARS-CoV-2 (Calu3), SARS-CoV-1 (Huh7), HCoV-229E (Huh7), HCoV-OC43 (BSC-1), H1N1 (A549), and EV-71 (RD) with or without 100μM z-VEID-fmk. Virus gene copy was quantified with RT-qPCR. f The half-maximal inhibitory concentrations (IC50s) of z-VEID-fmk on the replication of MERS-CoV (HFL), SARS-CoV-2 (Calu3), SARS-CoV-1 (Huh7), HCoV- 229E (Huh7) and HCoV-OC43 (BSC-1) in cell lysate and supernatant samples were determined with RT-qPCR and TCID50 assays, respectively (n=4 for HCoV-OC43 and EV-71, n=3 for other viruses). Data represented mean and standard deviations from the indicated number of biological repeats. Statistical significance between groups was determined with one way-ANOVA (d) or two way-ANOVA (b and e). * represented $p < 0.05$, ** represented $p < 0.01$, *** represented $p < 0.001$, **** represented $p < 0.0001$. ns = not significant. Bars in (a) represented 20μm.

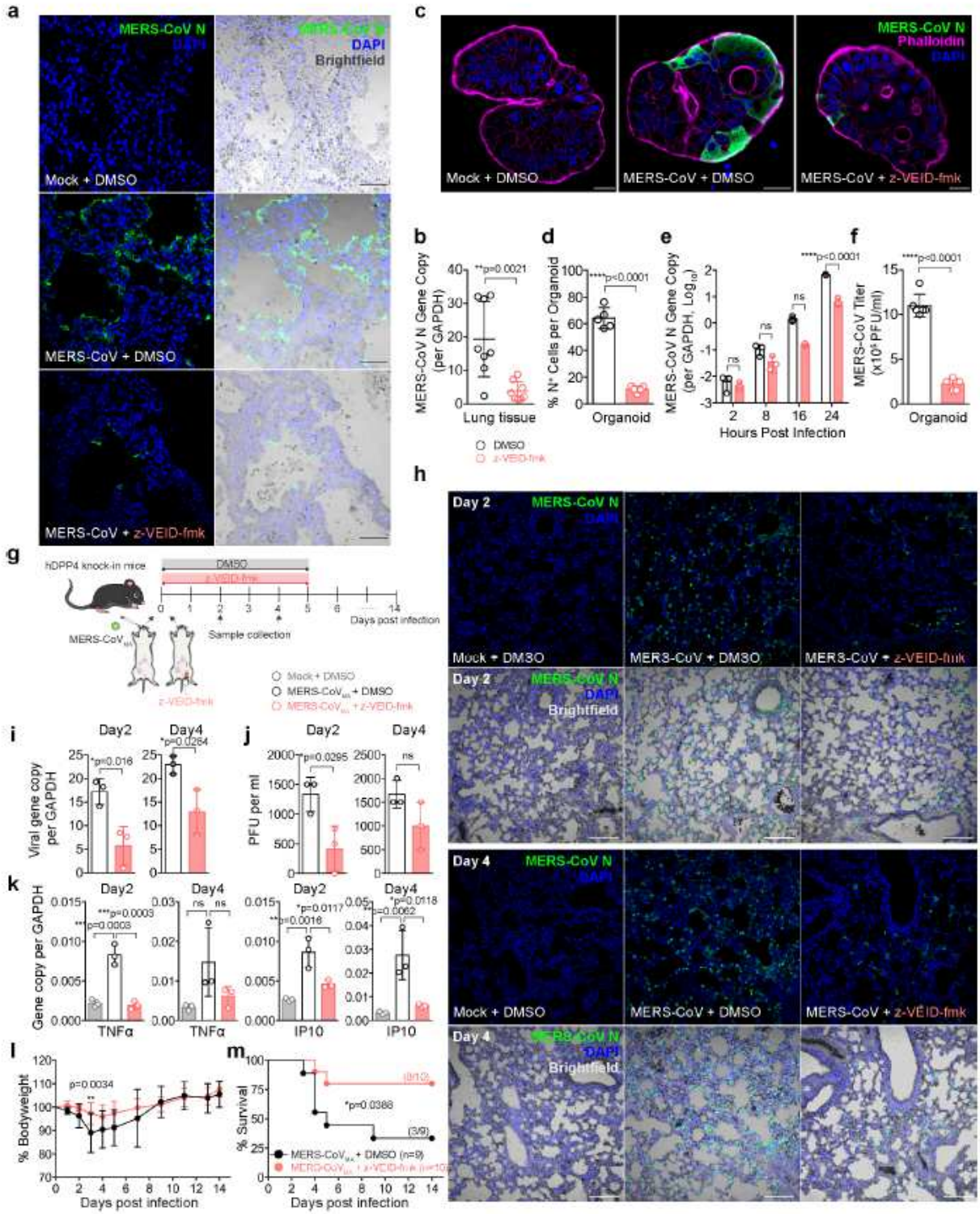

Figure 2

Caspase-6 inhibition attenuates MERS-CoV replication in human lung tissues, human intestinal organoids, and improves the survival of hDPP4 KI mice. a-b Ex vivo human lung tissues were infected with MERS-CoV and treated with z-VEID-fmk. The tissues and supernatants were harvested at 24 hpi for immunostaining with an in-house guinea pig immune serum against MERS-CoV N (a) and RT-qPCR (n=8) (b). c-f Human intestinal organoids were infected with MERS-CoV and treated with z-VEID-fmk. Organoids

were fixed at 24 hpi for immunostaining for N protein expression (c). The percentage of infected cells per organoids was calculated from counting the number of infected cells and uninfected cells per organoid (n=5) (d). N gene expression at the indicated time points was quantified with RT qPCR (n=3) (e). Infectious titer was determined with plaque assays (n=6) (f). g hDPP4 KI mice were intranasally inoculated with 2.5x103PFU MERS-CoVMA followed by intraperitoneal administration of 12.5mg/kg/day z-VEID-fmk or DMSO for 6 days or until sample harvest. h A subset of mice were harvested at day 2 and day 4 post infection. Mouse lungs were immunolabelled to detect MERS-CoV N expression. i Viral gene expression in mouse lungs were quantified with RT-qPCR (n=3). j Infectious titer was determined with plaque assays (n=3). k Expression of pro-inflammatory cytokines and chemokines were quantified with RT qPCR. l-m Body weight and survival of the infected mice were monitored for 14 days. Data represented mean and standard deviations from the indicated number of biological repeats. Statistical significance between groups was determined with one way-ANOVA (k), two way- ANOVA (e), Student's t-test (b, d, f, i, j, and l), or Log-rank (Mantel-Cox) test (m). * represented $p < 0.05$, ** represented $p < 0.01$, *** represented $p < 0.001$, **** represented $p < 0.0001$. ns = not significant. Bars in (a, c, and h) represented 50μm, 20μm, and 100μm, respectively.

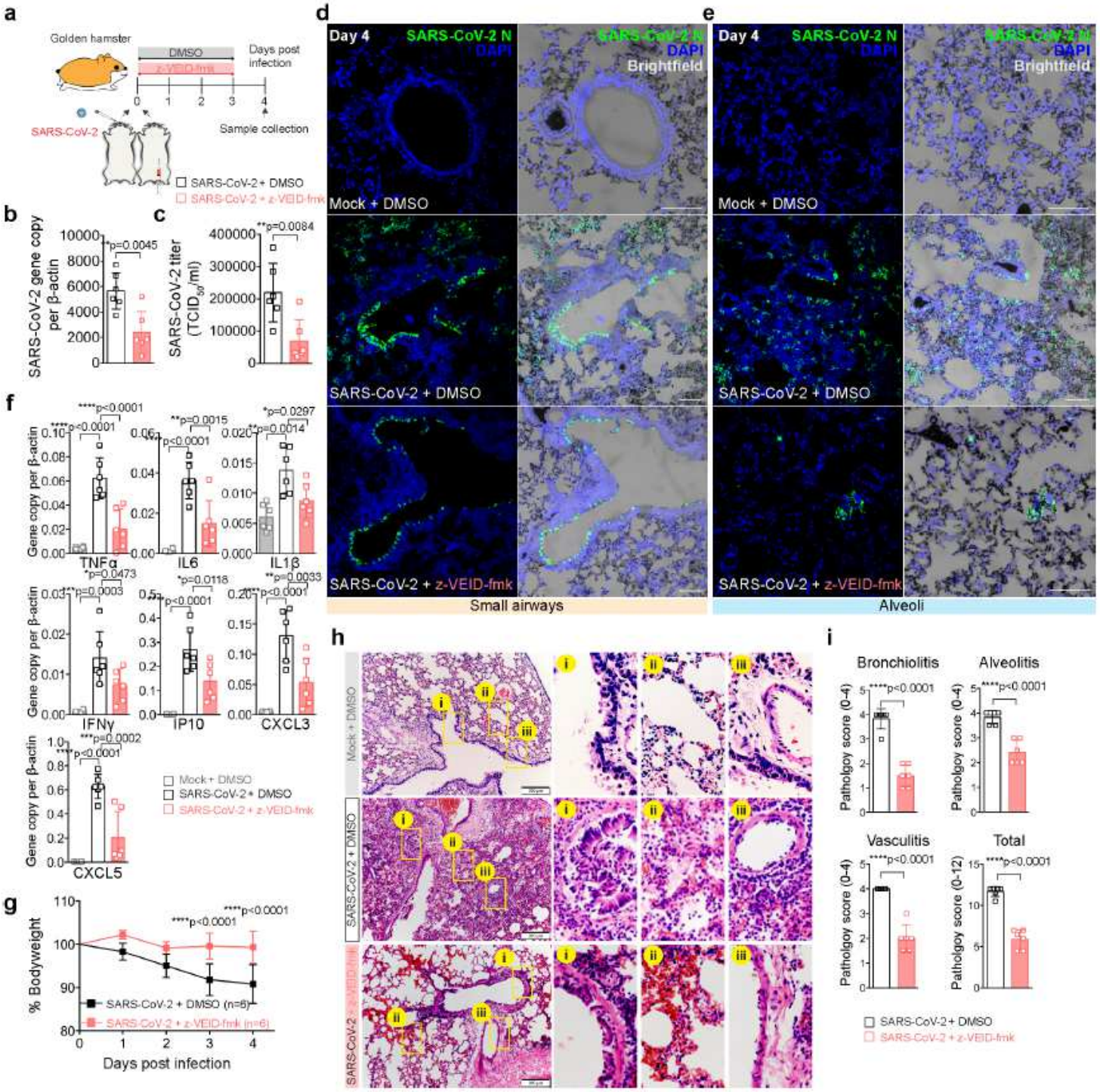

Figure 3

Caspase-6 inhibition ameliorates lung pathology and improves the body weight of SARS-CoV-2-infected golden Syrian hamsters. a Golden Syrian hamsters were intranasally inoculated with 3x103PFU SARS-CoV-2 followed by intraperitoneal administration of 12.5mg/kg/day z-VEID-fmk or DMSO for 4 days. b-c Hamsters were sacrificed at day 4 post infection, viral gene copy and infectious titer of hamster lungs were quantified with RT-qPCR and TCID50 assays, respectively (n=6). d-e Viral N protein expression in the small airways and alveoli of infected hamster lungs with or without z-VEID-fmk treatment was revealed

with immunofluorescence staining with the in-house rabbit immune serum against SARS-CoV-2 N. f Expression of pro-inflammatory cytokines and chemokines was quantified with RT-qPCR (n=6). g Body weight change of SARS-CoV-2-infected hamsters with z-VEID-fmk or mock treatment was documented from day 0 to day 4 post infection. h Representative images of haematoxylin and eosin (H&E) stained hamster lungs. (Top panels) mock-infected hamster lung sections showed normal histology, boxed areas were magnified showing (i) intact bronchiolar epithelium lining, (ii) thin alveolar wall and clear air sac, and (iii) a normal structure of pulmonary blood vessel section. (Middle panels) In SARS-CoV-2-infected hamsters, lung tissues showed diffuse inflammatory infiltration and exudation with disappearing air-exchange structures. Boxed areas were magnified to demonstrate the characteristic histopathological changes (i) peribronchiolar infiltration and bronchiolar epithelium desquamation, (ii) alveolar infiltration and haemorrhage with alveolar space filled with infiltrated immune cell and protein rich exudate, (iii) pulmonary blood vessel showed immune cells infiltration in the vessel wall, endothelium, and perivascular connective tissue. (Bottom panels) The hamster lung pathology was markedly improved with z-VEID-fmk treatment. Magnified images demonstrated (i) milder degree of immune cell infiltration in bronchiolar epithelium and peribronchiolar tissue, (ii) thickened alveolar wall with red blood cells but alveolar space showed no immune cell infiltration nor exudation, (iii) pulmonary vessel wall showed a few immune cells attached to the endothelium. i Quantitative scores for the lung histopathological changes of SARS-CoV-2- infected hamsters with or without z-VEID-fmk treatment. Three categories of characteristic histopathological changes including bronchiolitis, alveolitis and vasculitis were examined and scored. (n=6 and two-three lung lobes were examined from each hamster). Data represented mean and standard deviations from the indicated number of biological repeats. Statistical significance between groups was determined with one way-ANOVA (f) or Student’s t-test (b, c, g, and i). * represented $p < 0.05$, ** represented $p < 0.01$, *** represented $p < 0.001$, **** represented $p < 0.0001$. ns = not significant. Bars in (d and e) represented 100μm.

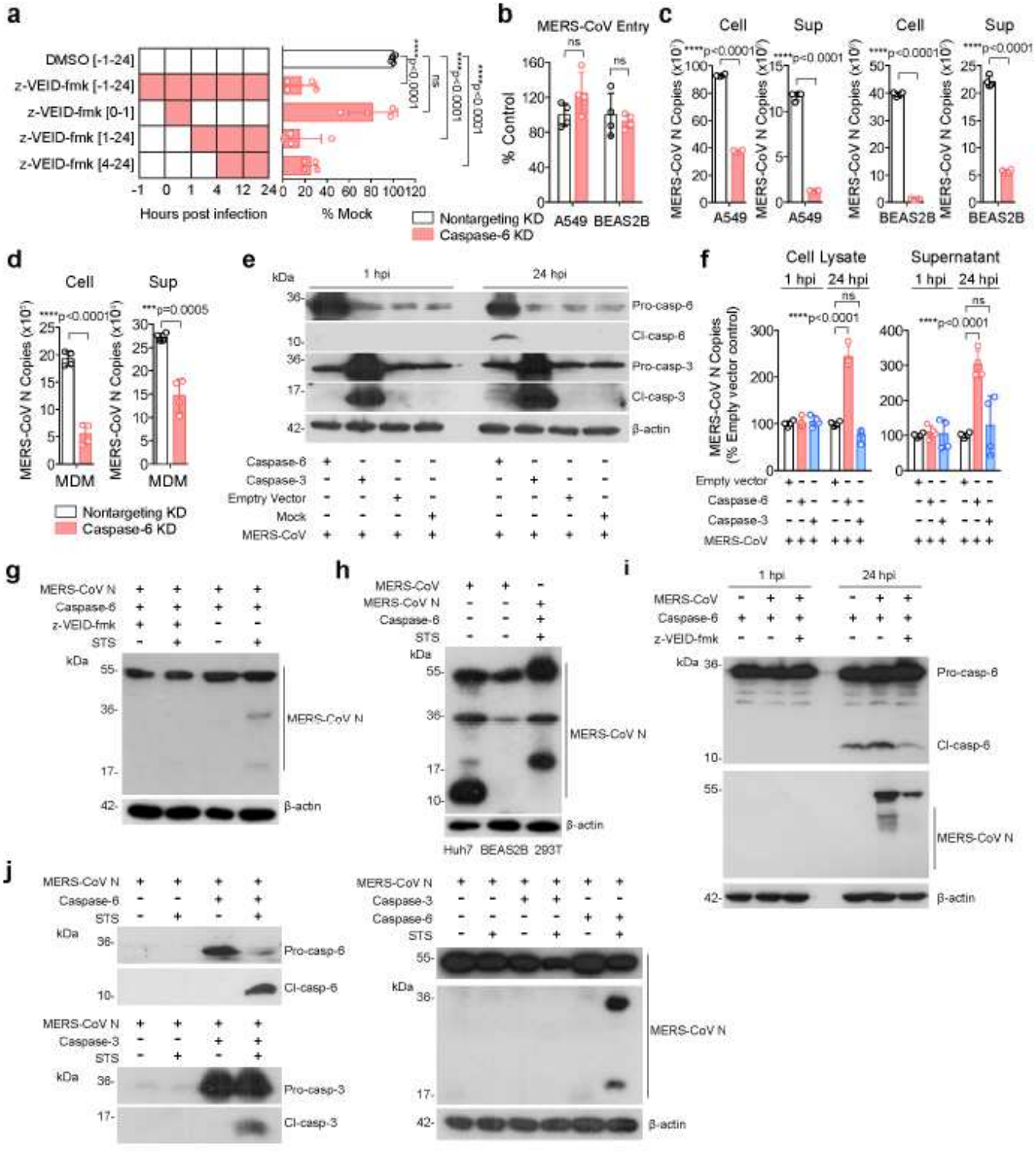

Figure 4

Caspase-6 modulates MERS-CoV replication at a post entry step and cleaves MERS-CoV N protein. a MERS-CoV-infected BEAS2B cells were incubated with z-VEID fmk in a time of addition assay. Virus gene copy in the supernatant was determined with RT qPCR at 24hpi (n=4). b-c Caspase-6 stable knockdown A549 and BEAS2B cells were infected with MERS-CoV at 0.1MOI. (b) Cell lysates were harvested at 1 hpi to quantify virus entry with RT-qPCR (n=4). (c) Virus replication at 24 hpi were quantified with RT-qPCR

(n=4). d MDMs were treated with caspase-6 or nontargeting siRNA and infected with MERS-CoV. Virus gene copy was quantified at 24 hpi (n=4). e-f Caspase-6- or caspase-3-overexpressed 293T cells were infected with MERS-CoV at 1MOI. Virus replication was quantified at 1 and 24 hpi with RT qPCR (n=4). g MERS-CoV N and caspase-6 were co-expressed in 293T cells with or without 100μM z-VEID-fmk. Cells were harvested for Western blot at 24 hours post transfection. 1μM staurosporine (STS) was added as an apoptosis trigger at 6 hours before sample harvest. h N cleavage in cell lysates from MERS-CoV-infected Huh7 and BEAS2B cells was compared to the N cleavage in cell lysates from MERS-CoV N and caspase-6 co-transfected 293T cells. i N cleavage in MERS-CoV-infected cells with or without z-VEID-fmk. j Comparison of MERS CoV N cleavage in caspase-6-overexpressed and caspase-3-overexpressed cells. Data represented mean and standard deviations from the indicated number of biological repeats. Statistical significance between groups was determined with one way-ANOVA (a), two-way ANOVA (b and f), or Student's t-test (c and d). * represented $p < 0.05$, ** represented $p < 0.01$, *** represented $p < 0.001$, **** represented $p < 0.0001$. ns = not significant.

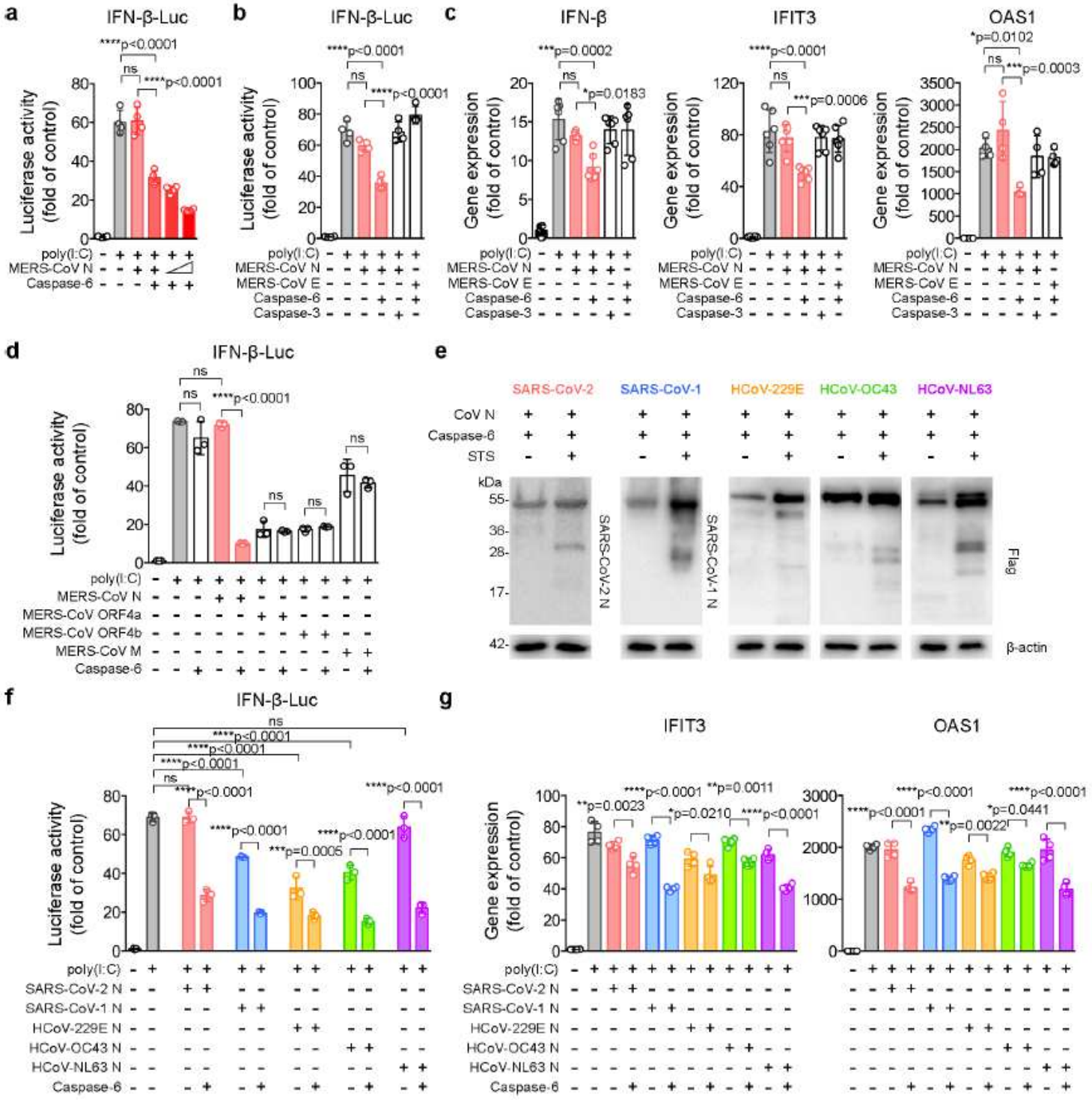

Figure 5

Caspase-6-mediated coronavirus N cleavage interferes with IFN signalling. a-b 293T cells were transfected with an IFN-β-Luc reporter plasmid, expression constructs of MERS-CoV N or E and caspase-6 or caspase-3, with or without poly(I:C). Cells were incubated for 24 hours before harvesting for dual-luciferase reporter assays (n=4). c 293T cells were transfected with the same set of plasmids. Gene expression of IFN-β, IFIT3, and OAS1 was quantified with RT-qPCR (n=6 for IFN-β and IFIT1, n=4 for

OAS1). d 293T cells were transfected with an IFN-β-Luc reporter plasmid, expression constructs of caspase-6 and MERS CoV N, ORF4a, ORF4b, or M, with or without poly(I:C). Cells were incubated for 24 hours before harvesting for dual-luciferase reporter assays (n=3). e N protein of the indicated coronaviruses were co-expressed with caspase-6. N cleavage was detected with Western blots. f 293T cells were transfected with an IFN-β-Luc reporter plasmid, expression constructs of caspase-6 and coronavirus N, with or without poly(I:C). Cells were incubated for 24 hours before harvesting for dual-luciferase reporter assays (n=3). g 293T cells were transfected with the same set of plasmids. Gene expression of IFIT3 and OAS1 was quantified with RT-qPCR (n=4). Data represented mean and standard deviations from the indicated number of biological repeats. Statistical significance between groups was determined with one way-ANOVA (a-f and h-i). * represented $p < 0.05$, ** represented $p < 0.01$, *** represented $p < 0.001$, **** represented $p < 0.0001$. ns = not significant.

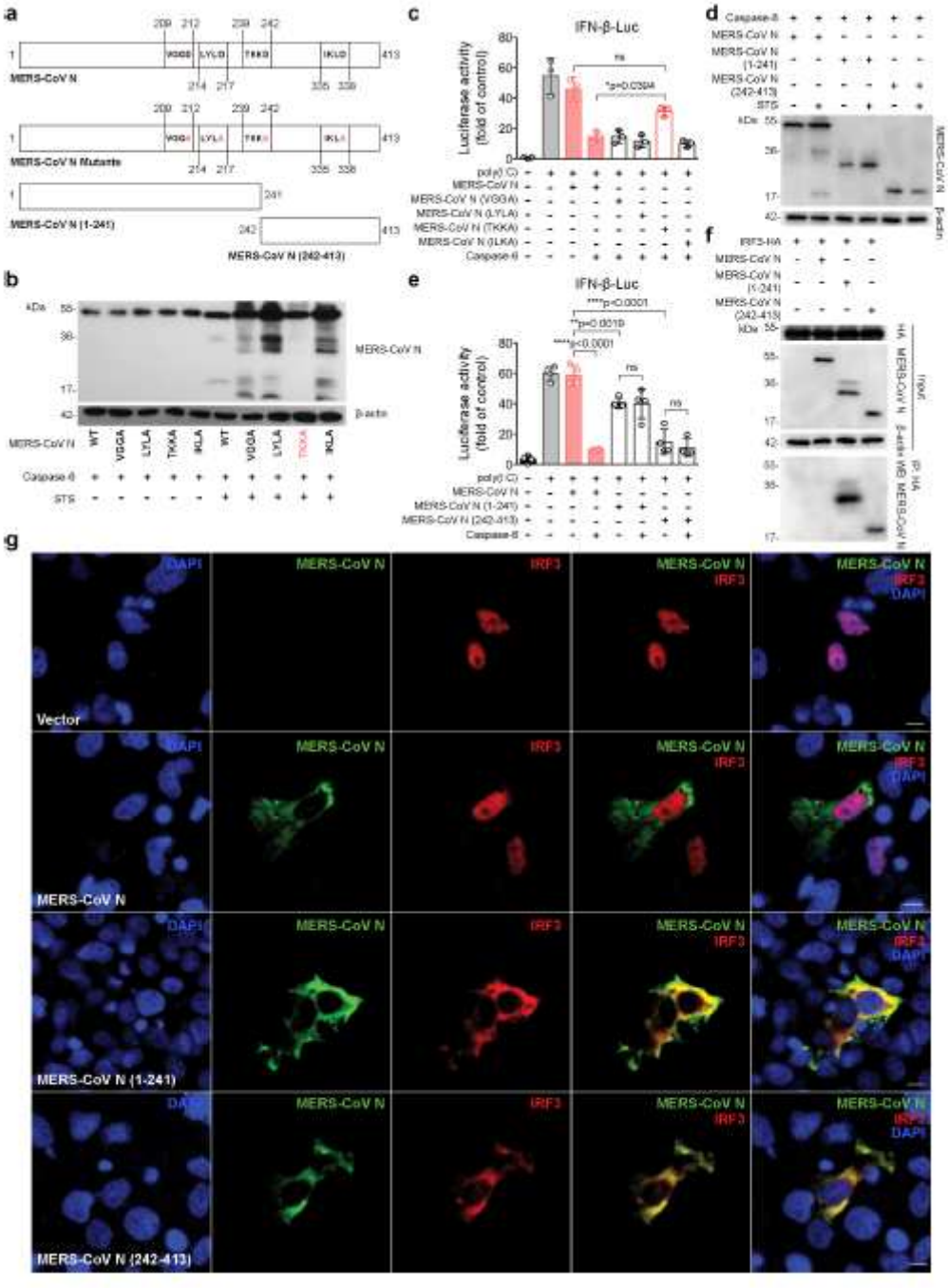

Figure 6

Caspase-6-mediated MERS-CoV N cleavage generates N fragments that block IRF3 translocation to the cell nucleus. a Schematic of N mutants. b Caspase-6-mediated cleavage of N mutants was evaluated with Western blots. c 293T cells were transfected with an IFN-β-Luc reporter plasmid, expression constructs of caspase-6 and MERS-CoV N or N mutants, with or without poly(I:C). Cells were incubated for 24 hours before harvesting for dual luciferase reporter assays (n=3). d Caspase-6-mediated cleavage of N, N(1-241), and N(242- 413) was evaluated with Western blots. e 293T cells were transfected with an IFN-β-Luc reporter plasmid, expression constructs of caspase-6 and MERS-CoV N, N(1-241), or N(242-413), with or without poly(I:C). Cells were incubated for 24 hours before harvesting for dual luciferase reporter assays (n=4). f Interaction between IRF3 and N, N(1-241), or N(242-413) was evaluated with co-immunoprecipitation assays using IRF3 as the bait protein. g 293T cells were transfected with expression constructs of IRF3, N, N(1-241), or N(242-413), and poly(I:C). Cells were fixed at 24 hours post transfection. Localization of N was detected with an in-house guinea pig anti-N immune serum and IRF3 was detected with a rabbit anti-HA antibody. Cell nuclei were identified with the DAPI stain. Data represented mean and standard deviations from the indicated number of biological repeats. Statistical significance between groups was determined with one way-ANOVA (c and e). * represented $p < 0.05$, ** represented $p < 0.01$, *** represented $p < 0.001$, **** represented $p < 0.0001$. ns = not significant. Bars in (g) represented 10μm.

Supplementary Files

This is a list of supplementary files associated with this preprint. Click to download.

- 20210304629AExtendedDataTable120210319.docx
- 20210304629AExtendedDataTable220210319.docx